CHEMICAL REVIEWS

Review

pubs.acs.org/CR

Insertion-Type Electrodes for Nonaqueous Li-Ion Capacitors

Vanchiappan Aravindan,*[,†] Joe Gnanaraj,*[,‡] Yun-Sung Lee,*[,§] and Srinivasan Madhavi*[,†,∥]

[†]Energy Research Institute @ NTU (ERI@N), Nanyang Technological University, Research Techno Plaza, 50 Nanyang Drive, Singapore 637553, Singapore

[‡]Yardney Technical Products, Inc., 2000 South County Trail, East Greenwich, Rhode Island 02818, United States

[§]Faculty of Applied Chemical Engineering, Chonnam National University, Gwang-ju 500-757, Korea

[∥]School of Materials Science and Engineering, Nanyang Technological University, Singapore 639798, Singapore

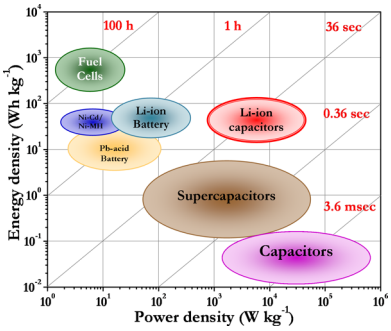

CONTENTS

1. INTRODUCTION

In the recent past, research focus is directed toward the development of high performance lithium ion (Li-ion) hybrid electrochemical supercapacitors (Li-HEC) because of their higher power density than the rechargeable battery (e.g., Li-ion batteries) and higher energy density than supercapacitors (e.g., electric double-layer capacitors, EDLC).[1−10] Thus, Li-HEC is expected to bridge the gap between the Li-ion batteries and EDLCs and become the ultimate power source for hybrid electric vehicles (HEV) and electric vehicles (EV) in the near future (Figure 1).[11] Apart from the mentioned applications, wind power generation, uninterruptible power sources, voltage sag compensation, photovoltaic power generation, CT and MRI scanners, and energy recovery systems in industrial machineries (forklift, cranes, power shovel) are worth mentioning. Before entering into the Li-HEC, a brief introduction about the EDLC and Li-ion batteries is necessary here.

On the basis of the energy storage mechanism, supercapacitors are classified into (i) EDLC and (ii) pseudocapacitors, irrespective of the electrolyte medium used (aqueous or nonaqueous). EDLC utilizes reversible electrochemical double layer capacitance obtained across the electrode/electrolyte interface (non-Faradaic process) where electric charges are accumulated on the electrode surface and ions of opposite charge are arranged in the electrolyte side.[12,13] Carbonaceous materials are favored as EDLC components due to their high specific surface area, relatively low cost, chemical stability in solutions irrespective of the pH value, ease of synthesis protocols with tailored pore size distribution and its amphoteric nature that allows rich electrochemical properties from donor to acceptor state, and a wide range of operating temperatures.[12,14] Various types of carbonaceous electrodes including allotropes (activated carbon, graphite, fullerenes, nanotubes, graphene, C_{60}), varied morphology (fibers, foams, fabrics), and

Special Issue: 2014 Batteries

Received: February 17, 2014
Published: July 10, 2014

   dx.doi.org/10.1021/cr5000915 | Chem. Rev. 2014, 114, 11619−11635

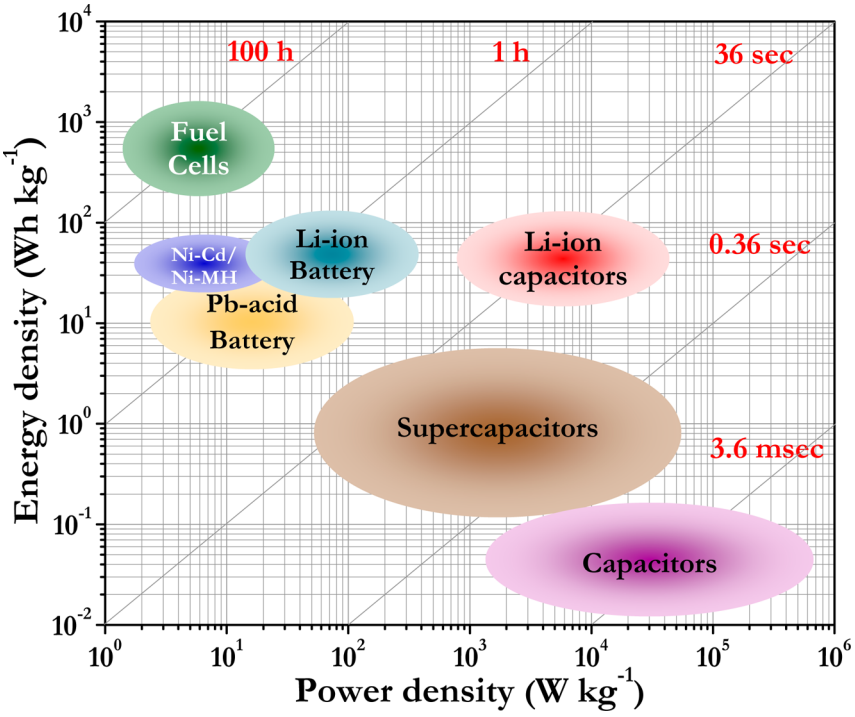

Figure 1. Ragone plot shows the demand for high power/energy electrochemical energy storage devices relative to present day technology.

microtextures have been extensively studied as EDLC component.[15] In addition, carbonaceous materials, particularly activated carbon (AC) with high surface area, which undergoes the formation of electric double layer, ensure the long-term cyclability over 10^6 cycles in aqueous medium. Poor cycle life of EDLC is noted in the case of organic electrolytes due to the higher equivalent series resistance (ESR); hence less studies have been carried out in nonaqueous medium.

In contrast to EDLCs, pseudocapacitors store charge Faradaically through the transfer of charge between electrode and electrolyte. This storage process is accomplished by electro-sorption, reduction−oxidation reactions, and intercalation processes as well. The combination reactions mentioned above (Faradaic process) enable one to achieve higher energy density and specific capacitance than the EDLC counterpart. Conducting polymers and transition metal oxides are the perfect examples for pseudocapacitive materials.[16] Among them, conducting polymers have a relatively high specific capacitance and electronic conductivity with relatively low ESR values and cost effectiveness as compared to carbonaceous electrodes. However, poor cyclability is the main concern for such conducting polymers. Similar to conducting polymers, transition metal oxides also showed lower ESR values and exhibited higher capacitance (e.g., amorphous ruthenium oxide, in which insertion and removal, or intercalation, of protons into its amorphous structure results in higher capacitance values), but higher cost and poor cyclability remain the serious issue for the commercialization of such transition metal oxides. In the application point of view, particularly to power the zero emission vehicles such as HEV and EV, both EDLC and pseudocapacitive materials are lacking in the energy density. Hence, to mitigate the relative disadvantages of EDLCs and pseudocapacitors to realize better performance characteristics, employing the concept of integrating both EDLC and Li-ion batteries has emerged and is called Li-ion hybrid electrochemical capacitor (Li-HEC) (Figure 2). The Li-HEC utilizes

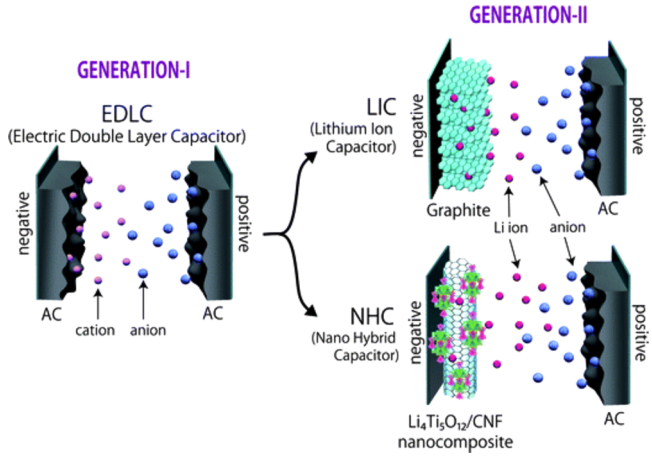

Figure 2. Generation-I is an ordinary electric double layer capacitor (EDLC) system that has a symmetric cell design utilizing activated carbon (AC) for both their positive and negative electrodes. Generation-II is an Li-ion-based hybrid supercapacitor (Li-HEC) with two typical representative asymmetric configurations. These are the hybrid systems employing a Faradaic Li-intercalating electrode and a non-Faradaic anion adsorption−desorption AC electrode. The Li-HEC is configured with prelithiated graphite/$LiBF_4$ or $LiPF_6$(PC)]/AC. The nanohybrid capacitor (NHC)/Li-HEC consists of an AC positive electrode combined with an ultrafast negative electrode made up of nanocrystalline $Li_4Ti_5O_{12}$, which effectively entangles with the nanocarbon matrix. Reprinted with permission from ref 3. Copyright 2012 The Royal Society of Chemistry.

both Faradaic and non-Faradaic processes to store charge to achieve higher energy density than EDLC and higher power density than Li-ion batteries without sacrificing cycling stability. Therefore, high surface area carbonaceous material is chosen as the capacitor-type electrode material (for non-Faradaic process) for Li-HEC by keeping long-term cyclability and cost effectiveness in mind. However, a high performance Li-

dx.doi.org/10.1021/cr5000915 | Chem. Rev. 2014, 114, 11619−11635

insertion-type electrode material is necessary to deliver high energy density during prolonged cycling. Unfortunately, only few materials have been explored as insertion-type electrode materials for Li-HEC applications with carbonaceous components.[17] Hence, the search for high performance Li-insertion-type electrode materials is desperately needed, and in this line we reviewed the materials tested for Li-HEC applications in nonaqueous medium. Current research activities on Li-HEC and future prospects of Li-insertion-type materials are described in detail.

Several insertion-type anode and cathode materials have been proposed to construct high performance Li-HEC with carbonaceous materials as counter electrode (Figure 3). In

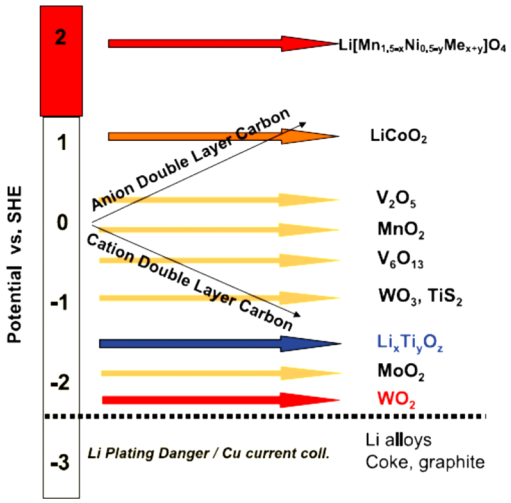

Figure 3. Schematic representation of three-electrode plot versus SHE. Plot shows relative potentials of the positive and negative electrodes of an activated carbon EDLC as a function of charge versus general redox potential of various intercalation compounds discussed in the text. Reprinted with permission from ref 4. Copyright 2005 Springer Science and Business Media.

contrast to non-Faradaic electrodes, insertion-type electrodes can accommodate Li-ions at various potentials with little variation in voltage as a function of state of charge. Proper utilization of insertion-type electrodes with optimized/balanced mass loading certainly leads to the substantial increase in the net operating potential and energy density as well.[4] Insertion-type compounds are very crucial to construct high performance Li-HEC, which has been opted not only dictated by the final operating potential, but side reactions while employing lower/higher voltage (vs Li) materials and possible deleterious electrochemical impact on other aspects of such nonaqueous charge storage system as a whole also have been considered.[4] Therefore, the following points should be considered before adopting the intercalation compound, which not only provides the enhancement in energy and power densities, but also translates exceptional robustness and safety features for Li-HEC.[4]

(i) Insertion electrodes, especially negative electrodes, must exhibit the operating potential over ~0.5 V vs Li, which is necessary for the use of Al-foil as current collector in Li-HEC assembly.[7] Below this potential, a Li_xAl alloy formation takes place, which in turn deteriorates the device performance. One the other hand, Ni and Cu substrates can also be used as current collectors, but the heaviness of the metals results in the decrease in specific energy density of the system.[4]

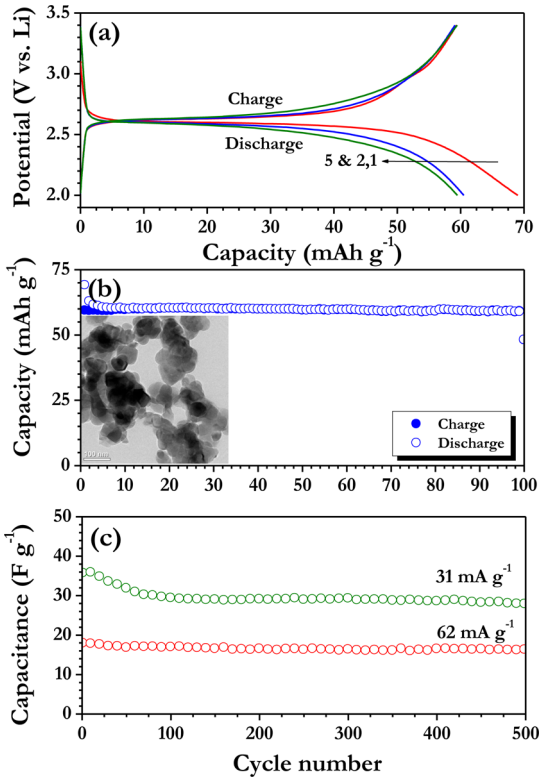

Figure 4. (a) Galvanostatic charge−discharge curves of Li/TiP_2O_7 half-cells cycled between 2 and 3.4 V vs Li at current density of 15 mA g^{-1}. (b) Plot of capacity versus cycle number of TiP_2O_7 in half-cell configuration. Inset: TEM pictures of combustion synthesized TiP_2O_7. (c) Plot of the specific discharge capacitance versus cycle number of AC/TiP_2O_7 Li-HEC at current densities of 31 and 62 mA g^{-1}. Reprinted with permission from ref 78. Copyright 2011 Elsevier.

(ii) Safe operational limit of the conventional carbonate-based electrolytes is between 1 and 4.5 V vs Li.[1] The testing potential below or above this limit certainly leads to the reduction or oxidation of the electrolyte solution, which in turn leads to irreversible consumption of Li. As a result, a thin solid electrolyte interface formation (SEI) takes place over the surface of the active particulates.[1] This SEI formation certainly increases the charge-transfer resistance and subsequently hampers the facile migration of Li-ions, which results in a detrimental effect on the power density of the system. Hence, the redox potential of insertion-type electrodes should not exceed this limitation.[4]

(iii) Unfortunately, the carbonate-based electrolytes (preferably EC, PC, DEC, and DMC) are exhibiting inferior ionic conductivities as compared to the solvent systems used in supercapacitors today.[7] Acetonitrile (AN)-based solutions are the best example for supercapacitor electrolytes, but such electrolytes are not stable at potentials <0.5 V vs Li, although they exhibit excellent performance in low temperature conditions.[4] As a consequence, the power density of the carbonate-based Li-HEC would be slightly lower than the expected level.

(iv) High current testing is the main issue for the insertion-type electrodes, either cathode or anode. Increasing current rates tends to increase the polarization of the electrodes.[18] Such polarization is the main issue for Li-HEC while operating at high current rates; for example, the insertion anode exhibits relatively lower operating potential (<0.4 V vs Li), which leads

dx.doi.org/10.1021/cr5000915 | Chem. Rev. 2014, 114, 11619−11635

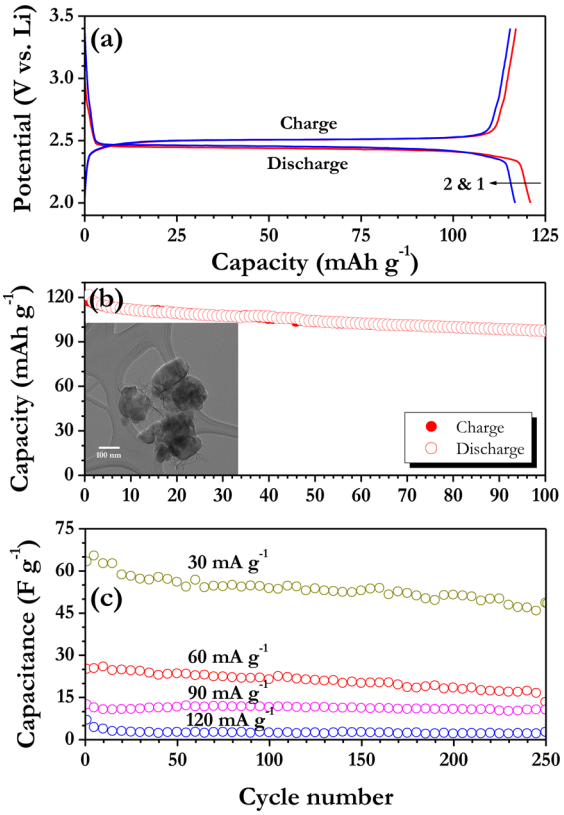

Figure 5. (a) Galvanostatic charge−discharge curves of Li/carbon-coated $LiTi_2(PO_4)_3$ half-cells cycled between 2 and 3.4 V vs Li at current density of 15 mA g^{-1}. (b) Plot of capacity versus cycle number of carbon-coated $LiTi_2(PO_4)_3$ in half-cell configuration. Inset: TEM pictures of carbon-coated $LiTi_2(PO_4)_3$ particles prepared by pechini-type polymerizable complex decomposition method. (c) Plot of the specific discharge capacitance versus cycle number of AC/carbon-coated $LiTi_2(PO_4)_3$ Li-HEC at various current densities. Reprinted with permission from ref 88. Copyright 2012 PCCP Owner Societies.

to the metallic reduction (Li°) of Li-ions and subsequent plating over the negative electrode as well.[4] Upon cycling, dendrite growth or mossy lithium formation resulted, which potentially shorts the cell as observed for the case of Li-ion cells.[19] This results in significant safety hazards on such nonaqueous Li-HEC while operating at high currents.

(v) Utilization of nanostructured materials as active electrodes can be beneficial for the betterment of high rate operations, which enables the facile diffusion of Li-ions, high surface to volume ratio, and good contact toward current collectors, thereby improving the power density of the Li-HEC system.[20]

(vi) In addition to the nanostructures, carbon coating over the active particles or making composites with carbonaceous materials improves the electrical conductivity, although such coating offers small reduction in volumetric capacity.

(vii) Non-Faradaic electrodes, that is, EDLC components, can store the charge through the use of double layer capacitance formed across the electrode/electrolyte interface and displayed extraordinary long cycle life (>500 000) due to the highly reversible nature of such double layer surface reaction.[4] To complement the performance of such electrode (example AC), insertion-type electrodes were highly anticipated to sustain similar full-depth of discharge cycles (>500 000).[4] This is 2 orders of magnitude greater than what has been reported to date for such insertion-type electrodes.

(viii) Li-HEC must be balanced for peak efficiency with respect to the specific capacity of the positive and negative electrodes. The choice of anion used in the electrolyte solutions is another important parameter. The "capacity" or ionic content of the electrolyte solution must be optimized to attain higher performance device.[5] This issue raises the importance of maximization of the salt solubility and also the selection of salts with minimal molecular weight. Specific capacity of Li-HEC also varies with lithium salts, for 176, 172, 252, and 286 mAh g^{-1} when $LiPF_6$, $LiCF_3SO_3$, $LiClO_4$, and $LiBF_4$, respectively, are used.[5] Hence, changing the salt from $LiPF_6$ to $LiBF_4$ will reduce the required weight of salt by 63% (because commercial Li-ion batteries comprise $LiPF_6$-based electrolyte solutions).[5] Because of the reversible consumption of the electrolyte salt in the solution, the molarity of electrolyte salt solution will undergo wide swings with each charge and discharge. Each mole of electrolyte is equivalent to 26.8 Ah in capacity. Therefore, in the development of such fast charging Li-HEC, one must be conscious of the change in conductivity of the electrolyte as a function of salt concentration. The conductivity of this system is a relatively strong function of electrolyte; therefore, the molarity of the solution should be optimized so that the change in the conductivity is minimized during cycling.

The operating mechanism of the electrolyte solution in Li-HEC contradicts with Li-ion battery chemistry. In Li-ion batteries, salt concentration polarization is a limiting factor to the rate capability of the electrolyte system. During fast discharge, Li-ions are extracted from the graphitic anodes and simultaneously inserted into transition metal cathodes. In contrast, Li-HEC has a symmetric driving force for the anions (PF_6^-) and cations (Li^+) to the opposing electrodes, which will reduce concentration gradients and result in a positive effect on the fundamental current density capability of the electrolyte system. This is especially apparent during fast discharge as both anions and cations are introduced into the electrolyte rather than depleted at one electrode like Li-ion batteries.

2. ANODES

Mass loading between the electrodes is necessary for the fabrication of Li-HEC to realize high energy density and power capability. Hence, the insertion-type electrode is used as the anode, and the counter electrode (carbonaceous materials) should be tested for the anion double layer formation (example PF_6^-, BF_4^-, etc.,) to balance the mass loading. More clearly, in single electrode configuration, the cell should be tested between open circuit potential and decomposition (oxidation) potential of the electrolyte, that is, 3−4.5 V vs Li or 3−4.6 V vs Li. In the mechanism, during charging, the cation in the electrolyte solution will be inserted into the host matrix and the presence of anion involving the double layer formation with carbonaceous electrodes will be used to sustain the charge neutrality of the electrolyte medium, and the reaction is reversed during the discharge process. The anodes are broadly classified into hydroxides, transition metal oxides, polyanions, and graphite.

2.1. Hydroxides

2.1.1. β-FeOOH. β-FeOOH is analogous to hollondite-type α-MnO_2, which has been investigated as a prospective high capacity cathode material for Li-ion batteries and can reversibly accommodate 1 mol of Li with theoretical capacity of ∼300 mAh g^{-1}.[21] Cheng et al.[22] reported the synthesis of β-FeOOH nanorods by conventional hydrothermal approach. β-FeOOH exhibited tetragonal phase with 2 × 2 tunnel-like structure,

dx.doi.org/10.1021/cr5000915 | Chem. Rev. 2014, 114, 11619−11635

which enables the facile insertion/extraction of Li-ions. At the current density of 0.5 mA cm^{-2}, half-cells (Li/β-FeOOH) delivered the initial discharge capacity of 237 and 200 mAh g^{-1} for the potential windows of 1.5−4.2 and 1.5−3.3 V vs Li, respectively. Capacity fading is noted irrespective of the potential windows tested for 50 cycles. Li-HEC is fabricated using β-FeOOH with optimized mass loading of AC and cycled between 0 and 3 V. The Li-HEC delivered good capacitance retention properties up to 800 cycles reported and found over ∼96% retention at 10 C rate. Further, the AC/β-FeOOH delivered the energy density of ∼45 Wh kg^{-1}, which is twice that of the AC/AC symmetric nonaqueous system.

2.2. Transition Metal Oxides

2.2.1. V_2O_5. V_2O_5 is considered a high capacity cathode material for Li-ion batteries due to the multiple oxidation states of V with theoretical capacity of >325 mAh g^{-1} (>2.2 mol of Li).[23−28] Usually beyond 2 mol of Li per formula unit is feasible; however, capacity fading is inevitable for such compounds. Several approaches have been adopted to improve the cyclability, including surface modification with carbon, carbon composite, and metal doping with various shapes and morphologies.[26] Among them, one-dimensional nanostructures are found noteworthy for the facile Li-insertion/extraction and accommodation of more Li-ions.[26] Restricted amounts of Li-ions are also possible to enhance the cyclability.[27] In this regard, electrospinning technique is adopted for the synthesis of one-dimensional V_2O_5 nanofibers (VNF) and exhibiting orthorhombic structure with *Pmmn* space group.[29] Half-cell, Li/VNF delivered the reversible capacity of ∼316 and ∼308 mAh g^{-1} in the second cycle at 0.1 C rate between 4 and 1.75 and 4−2 V vs Li, respectively. The capacity retention of ∼45 and ∼55% is noted after 50 cycles for the former and latter cases, respectively. Irrespective of the potential ranges, the half-cell experiencing the capacity fades during cycling as evidenced from Figure 6a and b. For the fabrication of Li-HEC, substrate free single walled carbon nanotube (SWCNT) network is used as positive electrode and VNF as anode cycled between 0 and 3 V. The Li-HEC, SWCNT/VNF renders the good cycling properties irrespective of the current density applied except for low current (30 mA g^{-1}) up to 500 cycles each current. SWCNT/VNF is able to deliver maximum energy and power densities of ∼18 Wh kg^{-1} and ∼315 W kg^{-1}, respectively.

2.2.2. α-MnO_2. MnO_2 is a unique material, which has been widely investigated as electrode material for both Li-ion battery and supercapacitor applications. Usually MnO_2 crystallizes in a wide range of crystal structures during the synthesis process.[30,31] Among them, hollondite-type structures are found noteworthy, and such α-MnO_2 nanorods are synthesized by hydrothermal route and exhibit tetragonal phase with *I*4/*m* space group.[32] The α-MnO_2 nanorods formed with tunnel structures (2 × 2) and their sizes are determined by the number of octahedral subunits. The half-cell delivered an initial discharge capacity of ∼130 mAh g^{-1} at a current density of 50 mA g^{-1} between 1.5 and 3.8 V vs Li. Li-insertion/extraction behavior is found to be a single phase reaction (Figure 8). Further, the cell exhibited stable capacity behavior and showed ∼90 mAh g^{-1} after 50 cycles. The Li-HEC is fabricated with AC as cathode and α-MnO_2 nanorods as anode and cycled between 0 and 3 V. AC/α-MnO_2 nanorods Li-HEC delivered the maximum energy and power densities of ∼9 Wh kg^{-1} and ∼87 W kg^{-1}. However, cyclability of AC/α-MnO_2 nanorods Li-HEC is found to be very poor in nonaqueous medium. Generally, the

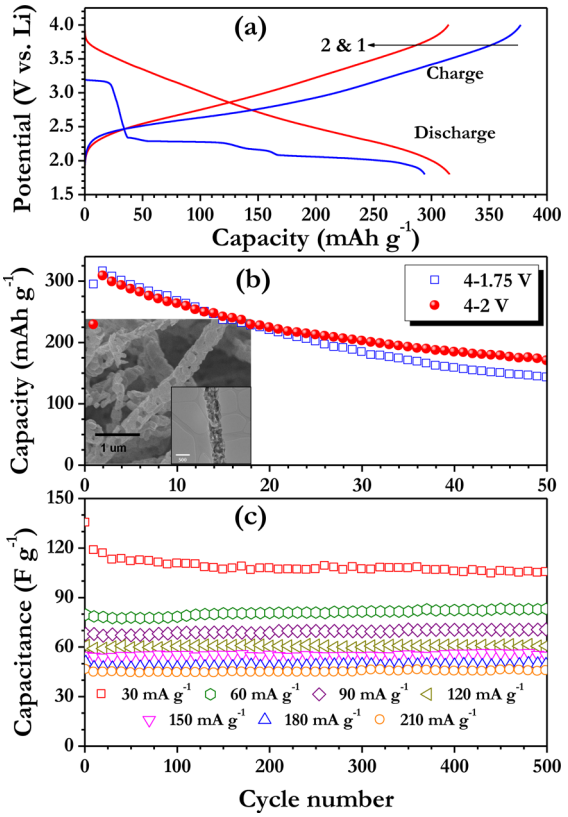

Figure 6. (a) Typical galvanostatic charge−discharge curves of Li/electrospun V_2O_5 half-cells cycled between 2 and 3.4 and 2−4 V vs Li at current density of 35 mA g^{-1}. (b) Plot of discharge capacity versus cycle number of electrospun V_2O_5 in half-cell configuration. Inset: SEM and TEM pictures of electrospun V_2O_5 nanofibers obtained by electrospinning. (c) Plot of the specific discharge capacitance versus cycle number of SWCNT/electrospun V_2O_5 Li-HEC at various current densities. Part (a) reprinted with permission from ref 25. Copyright 2011 Elsevier. Parts (b) and (c) reprinted with permission from ref 29. Copyright 2012 Wiley-VCH Verlag GmbH & Co. KGaA, Weinheim.

MnO_2-based supercapacitors are experiencing the capacitance fade irrespective of the electrolyte medium used and crystal structure. Wang et al.[33] fabricated Li-HEC using MnO_2/MWCNT as cathode and MWCNT as anode in the presence of 1 M $LiClO_4$ in EC:DEC (1/1 by vol) and tested between 0 and 2.7 V. Although Li-HEC delivered higher energy density (∼33 Wh kg^{-1}), it suffers from poor cyclability and power characteristics.

2.2.3. Anatase TiO_2. One of the most extensively studied polymorphs of TiO_2 is anatase phase, which has been evaluated as an insertion-type anode for Li-ion battery applications over a decade due to the overwhelming advantages of the highest theoretical capacity with less volume change during Li-insertion/extraction (∼3.7%). TiO_2 is abundant in the Earth's crust, environmentally benign, and of low cost, and expected to deliver highly durable cycling performance with much more safety features.[34−37] Unfortunately, the higher irreversible capacity loss (ICL) observed in the first cycle and higher operating potential (∼1.7 V vs Li) hinder the possibility of using them in practical Li-ion cells. However, the operating potential is favorable for the Li-HEC applications as insertion-type anode, but the huge irreversibility loss is the big issue, because electrolyte solution is the only source for Li-ions.

dx.doi.org/10.1021/cr5000915 | *Chem. Rev.* 2014, 114, 11619−11635

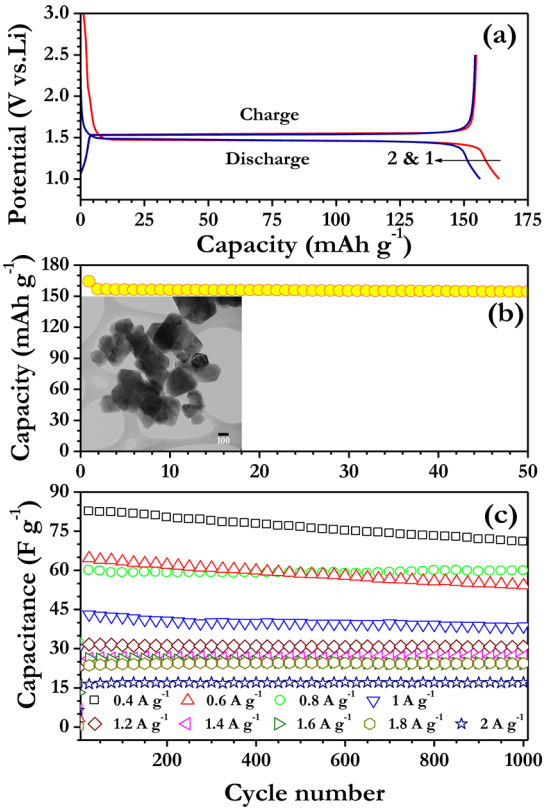

Figure 7. (a) Galvanostatic charge−discharge traces of Li/$LiCrTiO_4$ half-cells cycled between 1 and 2.5 V vs Li at current density of 15 mA g^{-1}. (b) Plot of discharge capacity versus cycle number of $LiCrTiO_4$ in half-cell configuration. Inset: TEM pictures of $LiCrTiO_4$ particles obtained by solid-state reaction method. (c) Plot of the specific discharge capacitance versus cycle number of AC/$LiCrTiO_4$ Li-HEC at various current densities. Reprinted with permission from ref 56. Copyright 2012 The Royal Society of Chemistry.

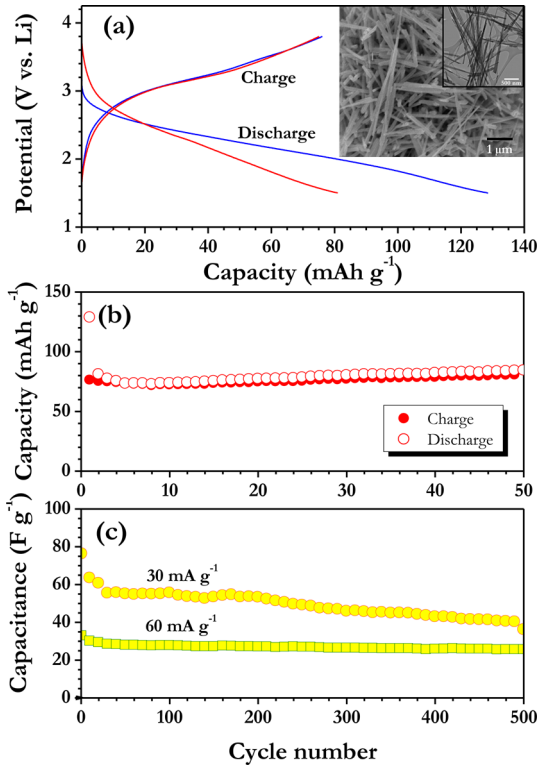

Figure 8. (a) Galvanostatic charge−discharge traces of Li/α-MnO_2 half-cells cycled between 1.5 and 3.8 V vs Li at current density of 50 mA g^{-1}. Inset: SEM and TEM pictures of α-MnO_2 particles obtained by hydrothermal route. (b) Plot of capacity versus cycle number of α-MnO_2 in half-cell configuration. (c) Plot of the specific discharge capacitance versus cycle number of AC/α-MnO_2 Li-HEC at various current densities. Reprinted with permission from ref 32. Copyright 2012 American Scientific Publishers.

Otherwise, the anatase TiO_2 phase should be prelithiated (similar to graphite) to avoid the consumption of Li. Therefore, no work has been carried out for such a fascinating anode. Recently, Kim et al.[38] reported the performance of anatase TiO_2-reduced graphene oxide (RGO) composite as anode and AC cathode between 1 and 3 V. The Li-HEC delivered the maximum energy and power densities of ∼42 Wh kg^{-1} and ∼8 kW kg^{-1}, respectively, with good cyclability of 10 000 cycles. However, the composite anode TiO_2 experienced the irreversible capacity loss of ∼75 mAh g^{-1} during half-cell studies. Later, Li-HEC was constructed using mesoporous anatase TiO_2 microsheperes with AC as reported by Cai et al.[39] and delivered the maximum energy density of ∼80 Wh kg^{-1}. Although anatase TiO_2 offers high energy density, the huge amount of Li-consumption in the first discharge is the main concern while employing the practical Li-HEC. Alternatively, a precharging can be utilized to avoid such irreversible capacity loss.

2.2.4. Bronze TiO_2. One of the best polymorphs suggested for the facile Li-insertion/extraction reaction was compared to anatase and rutile phases.[20] Interestingly, bronze phase (TiO_2-B) exhibited a lower Li-insertion potential (∼1.55 V vs Li) as compared to anatase phase (∼1.7 V vs Li), and less irreversible capacity loss was observed in the first cycle than in the anatase phase.[40] Unlike the multiple Li-insertion mechanism (solid-solution formation, two-phase reaction, and interfacial storage) observed in the anatase phase,[40,41] Li-insertion takes place in the two-phase reaction for the case of TiO_2-B.[42−48] A conventional hydrothermal route is adopted for the synthesis of TiO_2-B nanorods from the anatase phase under strong alkali hydroxide medium (15 M NaOH). Prepared monoclinic $Na_2Ti_3O_7$ nanorods are subjected to ion-exchange reaction with HCl to attain monoclinic $H_2Ti_3O_7$ phase and heat-treated at 450 °C to yield the desired phase (TiO_2-B).[49] The resultant TiO_2-B phase comprises a tunnel-like structure, which enables facile diffusion of Li-ions especially at high current rates. Therefore, a half-cell assembly is constructed (Li/TiO_2-B) and found the reversible insertion of ∼0.52 mol of Li at a high current rate of 100 mA g^{-1}. Further, the cell delivered good cyclability and retained ∼93% of reversible capacity after 200 cycles with operating potential of ∼1.5 V vs Li, which is almost similar to that of conventional $Li_4Ti_5O_{12}$ anodes (Figure 9). Li-HEC is fabricated with AC electrode under the optimized mass loadings and tested between 0 and 2.8 V for about 2000 cycles at a current density of 100 mA g^{-1}. Further, the electrochemical performance of electrospun PVdF-HFP membranes was also compared to conventional Whatman separators. The electrospun PVdF-HFP membranes comprising Li-HEC delivered the maximum energy and power densities of ∼23 Wh kg^{-1} and ∼2.8 kW kg^{-1}, respectively. The observed values are higher than the previous values reported by other researchers; for instance, Wang et al.[50] studied the performance of TiO_2-B nanowires with multiwalled carbon nanotube (MWCNT) cathodes that delivered the maximum energy density of

dx.doi.org/10.1021/cr5000915 | Chem. Rev. 2014, 114, 11619−11635

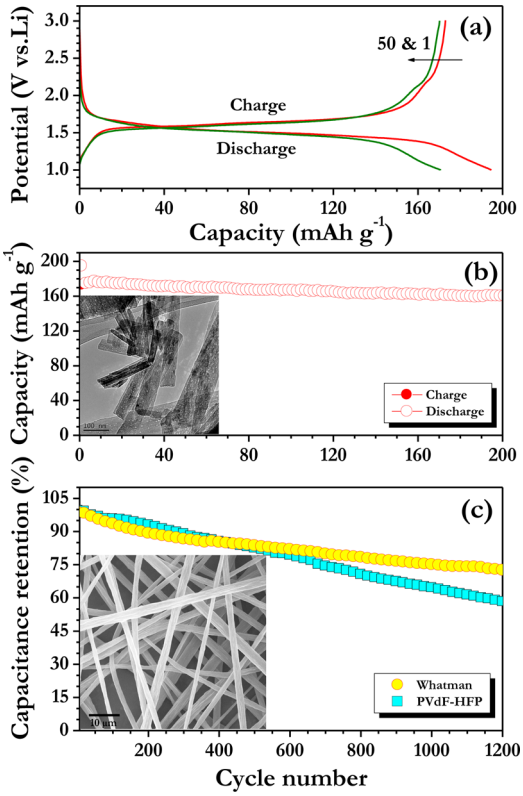

Figure 9. (a) Galvanostatic charge−discharge curves of Li/TiO_2-B half-cells cycled between 1 and 3 V vs Li at current density of 100 mA g^{-1}. (b) Plot of capacity versus cycle number of TiO_2-B in half-cell configuration. Inset: TEM pictures of TiO_2-B nanorods obtained by hydrothermal and subsequent ion-exchange method. (c) Plot of capacitance retention versus cycle number of AC/TiO_2-B Li-HEC at current density of 1.5 A g^{-1} with Whatman and electrospun PVdF-HFP membranes separator. Inset: SEM pictures of electrospun PVdF-HFP membranes. Reprinted with permission from ref 41. Copyright 2013 The Royal Society of Chemistry.

~12.5 Wh kg^{-1} without optimization of the electrodes, which results in less energy density, whereas TiO_2-B nanotubes delivered the maximum energy density of ~19.3 Wh kg^{-1} when coupled with MWCNT as positive electrode. Surprisingly, poor Li-insertion properties (0.35 mol of Li) are noted for the TiO_2-B bulk system (TiO_2-B powders); however, such system (AC/TiO_2-B) delivered the energy densities of ~45 and ~80 Wh kg^{-1} with various potential windows.

2.2.5. $Li_2Ti_3O_7$. Chen et al.[51] reported the synthesis of submicrometer-sized $Li_2Ti_3O_7$ particles by conventional sol−gel process at 1100 °C for 16 h in air atmosphere, exhibiting Ramsdellite structure with *Pnma* space group. In the half-cell assembly, it is apparent that the Li-insertion/extraction takes place more or less as a single phase reaction with operating potential of ~1.5 V vs Li and is able to accommodate ~1.55 mol of Li ($Li_{3.55}Ti_3O_7$) per formula unit. The observed values are lower than ~200 mAh g^{-1} (~1.7 mol of Li); see work by Villevieille et al.[52] and Cho et al.[53,54] Irrespective of the synthesis procedures employed for Li-insertion into Ramsdellite-type $Li_2Ti_3O_7$, good cyclability can be achieved in half-cell configuration. Li-HEC is constructed with AC cathode and tested between 1 and 3 V with meager capacitance fading in the initial cycles (~5%) and rendered good cyclability up to 500 cycles. The AC/$Li_2Ti_3O_7$ Li-HEC delivered maximum energy density of ~20 Wh kg^{-1} in ambient temperature conditions.

2.2.6. $LiCrTiO_4$. The performance of $LiCrTiO_4$ as anode is reported only in a few papers due to the toxicity and poor electrochemical profiles of Cr.[55−60] The reversible insertion of 1 mol of Li corresponds to the theoretical capacity of 157 mAh g^{-1}. Further, Li-insertion/extraction takes place according to the two-phase reaction mechanism with the operating potential of ~1.5 V vs Li, and an increase in volume change (0.7%) during Li-insertion is also noted. The operating potential of $LiCrTiO_4$ is the same as that of the well-known commercially available $Li_4Ti_5O_{12}$ anode, which makes the above candidate more attractive. High performance $LiCrTiO_4$ anodes are synthesized by conventional solid-state approach and exhibited pure phase spinel structure with $Fd\bar{3}m$ space group. The half-cell (Li/$LiCrTiO_4$) delivered the reversible capacity of ~155 mAh g^{-1} at a current density of 15 mA g^{-1}, which is very close to the theoretical capacity for insertion of 1 mol of lithium (Figure 7). Excellent cyclability is noted in half-cell configuration with capacity retention of ~98% after 50 galvanostatic cycles between 1 and 2.5 V vs Li. Li-HEC is fabricated with AC and $LiCrTiO_4$ as positive and negative electrodes, respectively. Li-HEC, AC/$LiCrTiO_4$ exhibited extraordinary cyclability irrespective of the current rates applied for about 9000 galvanostatic cycles (includes all of the current rates) and delivered energy and power densities of ~23 Wh kg^{-1} and ~4 kW kg^{-1}, respectively. The observed values are in very close proximity with commercially available $Li_4Ti_5O_{12}$-based systems.

2.2.7. $Li_4Ti_5O_{12}$. A spinel framework material comprising the general formula AB_2O_4 ($Li_4Ti_5O_{12}$ can also written as $Li(Li_{1/3}Ti_{5/3})O_4$) has been widely investigated as a promising and best insertion anode reported for Li-ion battery applications.[61,62] This is certainly possible for $Li_4Ti_5O_{12}$ anode because of its salient features as follows: (i) a first-order phase transition (two-phase reaction) is noted during the Li-insertion/extraction at ~1.55 V vs Li with thermodynamically flat profiles,[61,63,64] (ii) very high coloumbic efficiency (>95%) even at high current operations,[65] (iii) appreciable theoretical capacity ~175 mAh g^{-1} for reversible insertion of 3 mol of Li,[59,66] (iv) no unit cell volume variation is noted during Li-insertion/extraction (so-called "zero-strain" insertion host),[58] (v) no surface film formation (SEI layer) is evidenced,[61] (vi) easy synthesis protocol with low-cost raw materials, and (vii) environmental friendliness.[3,8,58,61,65−71] Amatucci et al.[5] first reported the demonstration of first prototype Li-HEC based on nanophase spinel $Li_4Ti_5O_{12}$ anode and AC cathode with three different electrolytes ($LiPF_6$/EC:DMC, $LiPF_6$/AN, and $LiBF_4$/AN). Among them, $Li_4Ti_5O_{12}$ anode and AC cathode comprising $LiPF_6$/AN delivered the maximum energy density of ~18 Wh kg^{-1} as compared to the $LiBF_4$/AN system (~11 Wh kg^{-1}). These results showed the slight reduction in energy density, which showed the contradiction that BF_4^- anions provide better capacitive properties than PF_6^- as suggested by same authors.[5] However, said configurations delivered a lack of power density, for example, with the $LiBF_4$/AN system capable of sustaining the ~4 kW kg^{-1}. Later, Naoi et al.[3,65,66,70] extended the studies, in which nanosized $Li_4Ti_5O_{12}$ particles have been attached with the CNF prepared by catalytic chemical vapor deposition. Anchoring of nanosized $Li_4Ti_5O_{12}$ particles enables the facile diffusion of Li-ions; that is, half-cell has been either charged/discharged within 12 s ($Li_4Ti_5O_{12}$/CNF is 70/30 ratio with mass loading of 1 mg). The charging/discharging protocol is equal to the 300 C rate and retains ~95% of initial reversible

dx.doi.org/10.1021/cr5000915 | *Chem. Rev.* 2014, 114, 11619−11635

capacity (~167 mAh g^{-1}). This extraordinary performance can provide the necessary enhancement in the power density prospective and delivered the maximum energy density of ~55 Wh kg^{-1} in the presence of 1 M $LiPF_6$ in EC:DEC (1:1 by vol) when AC is used as the counter electrode.[66] However, there is not much influence on the electrochemical performance of such configurations while changing the electrolyte into 1 M $LiBF_4$ in PC.[70] Irrespective of the electrolyte and applied current rate, the $Li_4Ti_5O_{12}$ anchored CNF delivered extraordinary cyclability of 15 000 cycles with ~90% retention of initial value.[3] Recently, $Li_4Ti_5O_{12}$ nanocrystals anchored super growth CNT (SGCNT) delivered even better Li-diffusion properties then CNF attached one. The $Li_4Ti_5O_{12}$/SGCNT (80:20 ratio) composite delivered the reversible capacity of ~78 mAh g^{-1} at 1200 C rate in half-cell configuration, whereas $Li_4Ti_5O_{12}$/CNF composite is able to deliver only ~30 mAh g^{-1} at this current rate. The observed energy density is 3 and 4.5 times higher than the $Li_4Ti_5O_{12}$/CNF and conversional EDLC configurations, respectively.[65] Recently, Ni et al.[72] reported the performance of in situ and ex situ carbon-modified $Li_4Ti_5O_{12}$ anode in Li-HEC configuration with AC electrode. AC/$Li_4Ti_5O_{12}$-C Li-HEC system delivered the maximum specific energy density of ~20 Wh kg^{-1} with capacity retention of ~84% after 9000 cycles at 32 C. Graphene-$Li_4Ti_5O_{12}$ composite anode has also been reported with a high energy of ~50 Wh kg^{-1} in the presence of AC counter electrode.[73] Chen et al.[74] and Jung et al.[75] also reported the performance of AC/$Li_4Ti_5O_{12}$ systems with improved gravimetric energy densities.

2.3. Polyanions

2.3.1. TiP_2O_7. Generally, pyrophosphate compounds offer a robust three-dimensional $(P_2O_7)^{4-}$ framework with multiple sites for alkali ions. A wide range of chemical stability, possible multidimensional ionic conduction channels, and richness in structural variation can hold potential for the discovery of next generation electrode.[59,76,77] Aravindan et al.[78] reported the synthesis of TiP_2O_7 nanoparticles by urea assisted combustion technique. The synthesized TiP_2O_7 nanoparticles exhibit cubic 3 × 3 × 3 super structure with $Pa\bar{3}$ space group. CV studies showed lithium insertion and extraction peaks are observed at ~2.54 and ~2.67 V vs Li in half-cell configuration (Li/TiP_2O_7) according to the two-phase reaction mechanism.[59] The observed first discharge capacity of ~69 mAh g^{-1} corresponds to the insertion of ~0.58 mol of Li per formula unit against the theoretical capacity of ~121 mAh g^{-1} (1 mol of Li). The typical galvanostatic cycling profiles are illustrated in Figure 4. However, the observed capacity is slightly less than the reported values in the literature.[59,79−81] The Li-HEC is fabricated with AC as cathode and TiP_2O_7 as anode in 1 M $LiPF_6$ in EC:DMC and tested between 0 and 3 V. The AC/TiP_2O_7, Li-HEC delivers an initial discharge capacitance of ~37 F g^{-1} at current density of 31 mA g^{-1}. Li-HEC, AC/TiP_2O_7 in the nonaqueous electrolyte showed good cycling profiles and delivered maximum energy and power densities of ~13 Wh kg^{-1} and ~371 W kg^{-1}, respectively, at room temperature.

2.3.2. $LiTi_2(PO_4)_3$. NASICON-type $LiTi_2(PO_4)_3$ powders have unique properties, which have the three-dimensional network and thereby enable high thermal stability in the lithiated/delithiated state, particularly PO_3^{2-}-based anions as compared to the rest of the spinel and layered-type materials. Further, $LiTi_2(PO_4)_3$ can be effectively used as anode, cathode, and electrolyte materials for Li-ion battery applications.[82−87] In this regard, NASICON-type submicrometer size $LiTi_2(PO_4)_3$ particles are synthesized via modified pechini-type polymerizable complex method.[88] Synthesized $LiTi_2(PO_4)_3$ particles are subsequently carbon-coated by the decomposition of glucose to yield the C-$LiTi_2(PO_4)_3$ powders and exhibit rhombohedral-hexagonal structure with $R\bar{3}c$ space group. The half-cell, Li/C-$LiTi_2(PO_4)_3$ delivered the initial discharge capacity of ~121 mAh g^{-1} (1.75 mol of Li) at current density of 15 mA g^{-1} and rendered the excellent capacity retention of ~83% initial discharge capacity after 70 cycles. These observed values are one of the best results reported on NASICON-type $LiTi_2(PO_4)_3$. In CV, well-defined Li-insertion and extraction potentials at ~2.4 and ~2.6 V vs Li reveal the two-phase reaction mechanism with theoretical capacity ~138 mAh g^{-1} for the insertion of 2 mol of Li. Figure 5 illustrates the electrochemical lithium insertion behavior. The Li-HEC is constructed with AC as cathode and $LiTi_2(PO_4)_3$ as anode in nonaqueous medium and cycles between 0 and 3 V at different current densities with optimized mass loading of the electrodes. Cycling profiles of AC/C-$LiTi_2(PO_4)_3$ Li-HEC are found inferior irrespective of the current rates applied, and it is due to the intrinsic nature of the NASICON-type anode. In addition, the Li-HEC AC/C-$LiTi_2(PO_4)_3$ delivered the maximum energy and power densities of ~14 Wh kg^{-1} and ~180 W kg^{-1}, respectively.

2.4. Graphite

Graphite is an allotrope of carbon, which has been predominantly used as an insertion-type anode for Li-ion power packs.[89−91] The concept of employing such graphite as cathode active materials was first proposed by Yoshio and co-workers[92] to develop high energy density EDLC or Megalo capacitors in the presence of 1 M $(C_2H_5)_4NBF_4$ in PC electrolyte solution. Later, Aida et al.[93] employed spherical shaped artificial graphite as anode for Li-HEC applications along with AC cathode in the wide operating potential of 1.5−4.3 V and achieved the energy density of ~81.8 Wh L^{-1} (EDLC shows only ~15.8 Wh L^{-1}). The influence of operating potential and mass loading of the electrodes is extensively investigated by Khomenko et al.[94] for AC/graphite Li-HEC. For such assembly, graphite is prelithiated before conducting the cell assembly. Stepwise charge and subsequent relaxation process is employed to improve the cyclability, and such procedure is called formation cycles. AC/graphite Li-HEC delivered good capacitance characteristics and retained ~60%, ~75%, and ~86% of initial capacity after 10 000 galvanostatic cycles at current density of 650 mA g^{-1} between 1.5−5, 1.5−4.7, and 1.5−4.5 V windows, respectively. Irrespective of the potential windows performed, a sudden drop of capacitance ~12% is noted for all three cases mentioned during prolonged cycling. Under the optimized conditions (1.5−4.5 V window), maximum energy density of ~103 Wh kg^{-1} is obtained for AC/graphite Li-HEC as compared to AC/AC EDLC (energy density of ~22.6 Wh kg^{-1}). Sivakumar and Pandolfo[95] also observed a similar trend using AC/graphite Li-HEC; in their case, maximum energy density of ~100 and ~55 Wh kg^{-1} is observed for 3.1−4.1 and 2−4.1 V windows, respectively, at 10 C rate. The authors concluded that prelithiation is a very important process to achieve good quality; uniform formation of SEI substantially provides extended calendar life. In addition, the SEI formation determines the cycle life of Li-HEC. The nature of the carbonaceous materials used as negative electrode and its influence in the electrochemical properties in Li-HEC configuration with AC cathode is reported by Kim et al.[96] Both

artificial and natural graphite-based Li-HEC delivered the maximum possible energy densities of ~125 Wh kg^{-1}, whereas hard carbon presented only ~85 Wh kg^{-1}. However, under harsh conditions (40 C rate), the Li-HEC based on hard carbons retained ~70% of initial capacity; however, both artificial and natural-based Li-HEC devices showed only ~26−29%. This excellent performance of hard carbon is believed to be the disordered microstructure composed of cross-linked carbon layers, which lead to facile Li-insertion/extraction processes. Cycling profiles clearly indicate the good capacitance retention characteristics for Li-HEC based on hard carbons (~83%), as compared to artificial and natural graphite after 10 000 galvanostatic cycles at 10 C rate between 1.5 and 3.9 V. Further, it is well established that the amorphous and isotropic texture of hard carbons is favorable for the fabrication of high power Li-ion power packs.[89] In the same line, hard carbons are also one of the more favorable candidates for the development of high power Li-ion capacitor as compared to graphitic anodes. However, electrolyte consumption or irreversible capacity loss during the first cycle is the main problem for such hard carbon-based electrodes. To circumvent the said issue, Cao and Zheng[97] reported the inclusion of stabilized lithium metal powders (SLMP) over the surface of the hard carbon electrodes (without prelithiation of the negative electrodes) and fabricated Li-HEC with AC cathodes. These SLMP supplied the Li-ions to hard carbon during Li-insertion/extraction reaction rather than Li-ions exclusively coming from the electrolyte solutions in conventional Li-HEC configuration. SLMP-deposited hard carbon-based Li-HEC delivered the maximum energy density of ~82 Wh kg^{-1}, whereas conventional hard carbon showed the energy density of ~25 Wh kg^{-1}. Excellent cyclability is noted for SLMP-deposited hard carbon-based Li-HEC for about 600 cycles with degradation of <3% drop in the initial value, whereas severe fading is noted for the conventional configuration because 1/3 of the Li-ions from the electrolyte are consumed by hard carbon (because there is no prelithium for both cases). Graphene nanosheets have been attractive as active high performance electrode material in the energy storage devices in the recent past. In this regard, Lee et al.[98] compared the electrochemical performance of AC, urea-reduced graphene oxide (URGO), and hydrazine reduced graphene oxide (HRGO) cathodes with prelithiated graphitic anodes in Li-HEC configuration between 2.2 and 3.8 V. The Li-HEC delivered the maximum energy density of ~106, ~74, and ~78 Wh kg^{-1} for prelithiated graphite with URGO, HRGO, and AC cathodes, respectively. Further, URGO/graphite Li-HEC delivered excellent cyclability for about 1000 cycles. The enhanced performance of URGO is mainly attributed to the presence of amide groups and its reversible reaction with Li-ions, which is better than hydroxyl group functionalized (HRGO) electrodes. Moreover, good adherence properties of the binder poly(acrylic acid) as compared to PVdF and PTFE cannot be ruled out under such harsh conditions. Although having certain advantages like high operating voltage, high energy density, long cycle life, and no thermal runway occurs as compared LIB, tedious prelithiation process and sharp charge−discharge curves that hinder one from obtaining the full range of energy spectrum, and poor rate capability are important issues to tackle.[99] Recently, JM Energy (JSR Micro) Corp. commercialized the prelithiated carbonaceous anode-based electrochemical energy storage device "ULTIMO" for a wide range of applications such as voltage sag compensator, wind power generation, forklift, LED lighting, etc., in either cells (laminate or prismatic) or modules.[100]

3. CATHODES

Similar to insertion anodes, mass balance between the electrodes is necessary to achieve high energy density Li-HEC. Here, the insertion-type electrode is used as cathode, and the counter electrode (carbonaceous materials) should be tested for the cation double layer formation to balance the mass loading. More clearly, in single electrode configuration, the cell should be tested between open circuit potential to decomposition (reduction) potential of the electrolyte, that is, 1.5−3 V vs Li. Accordingly, during the charge, the Li-ions are extracted from the cathode and involved in the cation double layer formation with carbonaceous electrode to maintain the charge neutrality in the electrolyte solution, whereas the mentioned reaction is reversed during the discharge process.[93] On the basis of the crystal structure, the cathodes are sectioned into layered oxides, spinel oxides, phosphates, fluorophosphates, and silicates.

3.1. Layered Oxides

3.1.1. $LiNi_{1/3}Mn_{1/3}Fe_{1/3}O_2$. Karthikeyan et al.[101] first explored the concept of employing composite cathode, that is, conducting polymers (polypropylene, PPy or polyaniline, PANI) with transition metal oxide as insertion-type electrode for Li-HEC assembly. Because it is well-known that $LiNi_{1/3}Mn_{1/3}Fe_{1/3}O_2$ is almost an insulating material, a conductive coating or composite with conducting material is essential to use in practical applications. A mixed hydroxide route is employed to prepare the phase pure layered-type $LiNi_{1/3}Mn_{1/3}Fe_{1/3}O_2$ electrodes. In situ chemical polymerization then is carried out to yield $LiNi_{1/3}Mn_{1/3}Fe_{1/3}O_2$−PANI/PPy composites and subsequently employed as electrode material for Li-HEC. In the half-cell assembly, $LiNi_{1/3}Mn_{1/3}Fe_{1/3}O_2$−PANI composite delivered the stable reversible capacity of ~181 mAh g^{-1} at 0.5 C rate (1 C is assumed as ~120 mAh g^{-1}). In addition, under harsh conditions (40 C), also the composite delivered the stable discharge capacity of ~110 mAh g^{-1}. Li-HEC is fabricated with AC as anode and $LiNi_{1/3}Mn_{1/3}Fe_{1/3}O_2$−PANI as cathode and cycled between the 0 and 3 V range. The $LiNi_{1/3}Mn_{1/3}Fe_{1/3}O_2$−PANI/AC delivered the maximum energy density of ~49 Wh kg^{-1}, whereas PPy composites delivered ~18 Wh kg^{-1}. However, bare material delivered only ~10 Wh kg^{-1}. Irrespective of the energy densities, Li-HEC rendered excellent cyclability for about 5000 galvanostatic cycles with retention of over ~90% for PANI- and PPy-based composites.

3.1.2. $LiNi_{1/3}Mn_{1/3}Co_{1/3}O_2$. Because of the restricted delithiation of $LiCoO_2$ during electrochemical cycling, the concept of using layered-type mixed metal oxides with high capacity of over 200 mAh g^{-1} has been proposed as cathode active material for Li-ion batteries by Ozhuku et al.[102] Since then, several research works are devoted to developing such high performance cathode and approaching commercialization. Comparison and performance of $LiNi_{1/3}Mn_{1/3}Co_{1/3}O_2$ cathodes for Li-HEC applications prepared through carbonate and hydroxide coprecipitation techniques are reported by Yoon et al.[103] The $LiNi_{1/3}Mn_{1/3}Co_{1/3}O_2$ prepared by the carbonate-based coprecipitation technique delivered the maximum reversible capacity of ~160 mAh g^{-1} at 0.2 C rate. At high current rate (1.6 A g^{-1}), $LiNi_{1/3}Mn_{1/3}Co_{1/3}O_2$ delivered the specific capacitance of ~249 and ~195 F g^{-1} for carbonate and

dx.doi.org/10.1021/cr5000915 | Chem. Rev. 2014, 114, 11619−11635

hydroxide coprecipitation techniques, respectively. The Li-HEC is fabricated with AC anode and tested between the range of 0−2.2 V in ambient temperature conditions. The Li-HEC $LiNi_{1/3}Mn_{1/3}Co_{1/3}O_2$/AC delivered the specific capacitance of ∼60 and ∼50 F g^{-1} for carbonate and hydroxide coprecipitation techniques, respectively, which is higher than the AC/AC EDLC configuration (27 F g^{-1}). Further, $LiNi_{1/3}Mn_{1/3}Co_{1/3}O_2$/AC retained the capacitance retention of over 94.8% for carbonate-based coprecipitation technique as compared to the hydroxide precipitation (88.4%) process after 500 cycles.

3.1.3. Li_2MoO_3. This is one of the high capacity cathodes employed for Li-ion batteries due to the multiple oxidation states of Mo; however, due to the poor electrochemical performance, it has been eliminated as a promising active material. Usually Li_2MoO_3 exhibits rhombohedral symmetry, which is close to the α-$NaFeO_2$ structure with theoretical capacity of 340 mAh g^{-1} for two electron reactions.[104] However, the synthesis temperature strongly influences the electrochemical properties of Li_2MoO_3, which is clearly observed from Kobayashi et al.'s[105] work. Interestingly, usage as additive along with electro-active materials such as $LiCoO_2$ cathodes is found excellent due to the higher thermal stability in the charged state and the ability to form a wide range of solid solutions.[106] Park et al.[107] adopted the same concept of employing them as additive along with AC in the Li-HEC, while hard carbon acts as the counter electrode. The incorporation of Li_2MoO_3 with AC electrode alleviates the prelithiation of hard carbon. Increasing the Li_2MoO_3 concentration (0 to 10 wt %) leads to the increase in irreversible capacity in the Li-HEC configuration, because the half-cell assembly of Li_2MoO_3 shows huge irreversibility in the first cycle. The Li-HEC is cycled between 1.5 and 3.9 V and delivered the discharge capacitance of ∼0.5 F as compared to ∼0.39 F for conventional Li-HEC comprising AC anode and prelithiated hard carbon cathode. Coloumbic efficiency was also found superior for Li_2MoO_3 doped AC (∼86.7%) as compared to AC (∼64.6%) in the first cycle. This huge difference between the two electrodes is mainly due to the efficiency of lithium ion extraction after lithium doping. Further, kinetically favorable characteristics of Li_2MoO_3 arising from its stable structure during cycling cannot be ruled out. Good cyclability for both configurations is noted for about 200 cycles at 10 C rate with retention of ∼92% and ∼94.5% of initial capacitance retention for Li_2MoO_3 doped AC and native AC comprising configurations, respectively. Recently, Park et al.[108] reported the performance of Li_2RuO_3 codoped Li_2MoO_3/AC composite as positive electrode and hard carbon as negative electrode, but only marginal increasing energy density was noted.

3.2. Spinel Oxides

3.2.1. $LiMn_2O_4$. Spinel phase $LiMn_2O_4$ is considered as a promising 4 V greener cathode material for Li-ion battery applications and was also investigated extensively for Li-HEC applications.[109−112] Ma et al.[113] first reported the performance of Li-HEC comprising $LiMn_2O_4$ as cathode along with Birnessite-type manganese dioxide (MnO_2)/MWCNT (37%) as composite anode in 1 M $LiClO_4$ in PC electrolyte solution. The Li-HEC is cycled between 0 and 2.5 V and delivered maximum energy and power density of ∼56 Wh kg^{-1} and ∼2.4 kW kg^{-1}, respectively. Cericola et al.[114,115] reported the performance of $LiMn_2O_4$-based Li-HEC in bimaterial electrode configurations by varying the mass ratio and C rate. The $LiMn_2O_4$/AC Li-HEC system delivered higher energy (∼45 Wh kg^{-1}) density than the conventional AC/$Li_4Ti_5O_{12}$ system (∼30 Wh kg^{-1}) in the conventional internal series hybrid configuration, whereas power density is restricted to ∼1.2 kW kg^{-1}.[116] However, the parallel hybrid system $LiMn_2O_4$/AC//AC/$Li_4Ti_5O_{12}$ delivered the specific energy density of ∼56 Wh kg^{-1} with maximum power capability of ∼27 kW kg^{-1}. Nevertheless, Hu et al.[117] reported the performance of $LiMn_2O_4$−AC composite electrodes to yield high energy and power capability with $Li_4Ti_5O_{12}$ anodes by varying the AC concentrations (hybrid battery−capacitor configuration). Further, the influence of the charging condition, that is, constant current (CC) and constant current−constant voltage (CC−CV), was also studied for the said configuration in which the CC−CV mode is found appealing. Li-HEC comprising $0.3LiMn_2O_4$−$0.7AC/Li_4Ti_5O_{12}$ delivered maximum energy density of ∼16.5 Wh kg^{-1} and rendered good cycling capability of ∼96% capacitance retention after 2500 cycles in CC−CV mode.

3.2.2. $LiNi_{0.5}Mn_{1.5}O_4$. Ni doped spinel $LiNi_{0.5}Mn_{1.5}O_4$ is extensively studied as 5 V cathode materials for Li-ion battery applications.[118−121] Li et al.[122] first employed this as cathode active material for Li-HEC applications along with AC as counter electrode. The active materials are synthesized by the poly(vinyl alcohol)-mediated sol−gel process. The synthesized spinel phase $LiNi_{0.5}Mn_{1.5}O_4$ comprised only Mn^{4+} ions and delivered the reversible capacity of ∼125 mAh g^{-1} with a long distinct plateau around ∼4.7 V vs Li. The Li-HEC is fabricated with the mass loading of 1:3 ratio for $LiNi_{0.5}Mn_{1.5}O_4$ and AC electrodes, respectively. The hybrid device is cycled between 0 and 2.8 V and a delivered maximum specific energy density of ∼55 Wh kg^{-1}. Further, $LiNi_{0.5}Mn_{1.5}O_4$/AC Li-HEC delivered excellent cyclability at 10 C rate and retained 80% of initial discharge capacitance between 1.5 and 2.8 V. Later, Wu et al.[123] reported the performance of spinel phase $LiNi_{0.5}Mn_{1.5}O_4$ by modified solid-state method, which comprising a trace amount of Mn^{3+} ions, which was clearly evidenced from the galvanostatic charge−discharge profiles. The half-cell, Li/$LiNi_{0.5}Mn_{1.5}O_4$, delivered the reversible capacity of ∼132 mAh g^{-1} in ambient temperature conditions. Li-HEC is assembled with optimized mass loading of the electrodes (1:3 for cathode to anode) and delivered a maximum energy density of ∼56 Wh kg^{-1}. Further, $LiNi_{0.5}Mn_{1.5}O_4$/AC Li-HEC demonstrated good cyclability of about 1000 cycles with capacitance retention of ∼95% at current density 20 mA cm^{-2}. Typical charge−discharge curves of $LiNi_{0.5}Mn_{1.5}O_4$/AC Li-HEC at different current densities are shown in Figure 10.

3.3. Phosphates

3.3.1. $LiFePO_4$. Electrochemical activity of olivine phase $LiFePO_4$ was first reported by Padhi et al.;[124] thereafter, several works have been reported for this material as cathode for Li-ion batteries and recently commercialized by A123 systems, K2 Energy, and Sony Inc.[125] Olivine phase $LiFePO_4$ exhibits a flat discharge profile (∼3.4 V vs Li), good thermal stability in both lithiated and delithiated state, high theoretical capacity (170 mAh g^{-1}), and environmentally friendly properties.[126−129] The performance of olivine phase $LiFePO_4$ nanoparticles embedded on nanoporous carbon matrix as positive electrode in Li-HEC configuration along with AC electrode was reported by Wu et al.[130] Supercapacitor measurements were carried out between 0 and 2.8 V at a current density of 6.8 A g^{-1} and compared to the AC/AC symmetric system under the same testing conditions.

dx.doi.org/10.1021/cr5000915 | Chem. Rev. 2014, 114, 11619−11635

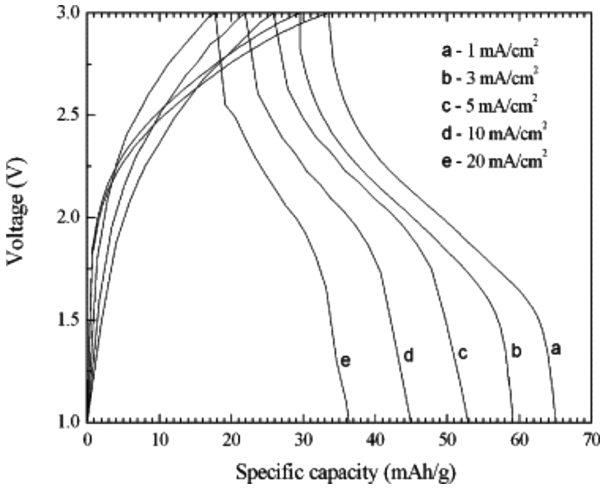

Figure 10. Charge/discharge curves of the $LiNi_{0.5}Mn_{1.5}O_4$/AC hybrid supercapacitor at different discharge current densities in 1 M $LiPF_6$ in EC/DMC electrolyte between 1.0 and 3.0 V. Reprinted with permission from ref 123. Copyright 2009 Elsevier.

Unfortunately, no detailed study has been reported. Chen et al.[131] reported the influence $LiFePO_4$ concentration on the electrochemical performance of the AC_{1-x}–xLiFePO$_4$/$Li_4Ti_5O_{12}$ Li-HEC system. An 80 wt % of $LiFePO_4$ and 20 wt % of AC showed 53% higher specific capacity than the AC/$Li_4Ti_5O_{12}$ system and delivered good cyclability as well. The observed energy density for said composition is (~63 Wh kg^{-1}) found higher than that of the conversional AC/$Li_4Ti_5O_{12}$ system (10–15 Wh kg^{-1}). Hu et al.[132,133] also investigated the role of AC concentration in Li-HEC configuration toward $Li_4Ti_5O_{12}$. Recently, Na et al.[134] reported the performance of AC_{1-x}–xLiFePO$_4$/MCMB systems cycled between 2 and 4 V. 30% of AC comprising system delivered the maximum energy density of ~69 Wh kg^{-1} with good capacity retention of about 100 cycles.

3.3.2. $LiCoPO_4$. One of the high voltage cathodes (~4.8 V vs Li) employed for Li-ion battery applications belongs to the olivine framework materials. The operating potential is higher than conventional carbonate-based electrolyte solutions.[135,136] Aurbach et al.[137,138] found that the dissolution of polyanion $(PO_3)^-$ group in the conventional solutions provides the setback in this material research. Apart from the various synthesis procedures employed, alternate approaches like carbon coating, Co site doping, and preparation of Li-rich and deficient phases have also been investigated to enable good conductivity toward conventional solutions.[139−142] Polyol (polyethylene glycol)-mediated approach is employed to synthesize high voltage olivine phase $LiCoPO_4$ nanoparticles for different calcination durations at 800 °C by Vasanthi et al.[143] Among them, single phase $LiCoPO_4$ nanoparticles are obtained for 2 h sintering duration and delivered the discharge capacity of ~40 mAh g^{-1}, which corresponds to the insertion of ~0.24 mol of Li. Li-HEC is fabricated with carbon nanofoams (CNf surface area of 1500 m^2 g^{-1}) as anode with 1 M $LiClO_4$ in EC/PC as electrolyte solution. In single electrode configuration, specific capacitance of ~55 and ~30 F g^{-1} is noted for $LiCoPO_4$ and CNf, respectively. Li-HEC is constructed with optimized mass loadings and tested between 0 and 2 V at ambient conditions. Li-HEC delivered maximum energy and power densities of ~2.9 Wh kg^{-1} and ~0.19 kW kg^{-1}, respectively. However, $LiCoPO_4$ treated for 4 h (contains impurities of Co_3O_4 and Li_3PO_4) delivered energy density of ~112.9 Wh kg^{-1} and retained ~67% capacity after 1000 cycles, whereas phase pure material rendered only ~60% capacitance retention. This higher energy density is due to pseudocapacitance offered by the impurity phase Co_3O_4.

3.4. Fluorophosphates

3.4.1. Li_2CoPO_4F. This is one of the high voltage cathode materials recently attracted by researchers because of the presence of highly electronegative F^- ions, which provide much more stability than their counterpart oxygen ions, preferably $LiCoPO_4$.[144] These fluorophosphate materials possess a 3D-framework structure in which the M–F bonds have higher ionicity than M–O bonds, and hence the $M^{n/n+1}$ redox couple is expected to exhibit a higher potential than phosphates.[144,145] During electrochemical cycling, cathode Li_2CoPO_4F undergoes single phase Li-insertion/extraction process rather than the first-order phase transition (two-phase reaction) noted for parent compound $LiCoPO_4$.[144,146] However, capacity fading during cycling is inevitable because of the high voltage redox couple of $Co^{2+/3+}$. For the same reason, the removal of second Li-ion is highly restricted.[135,144] Recently, Karthikeyan et al.[145] reported the possibility of using such high voltage cathode in Li-HEC configuration along with AC anode. The cathode delivered the reversible capacity of ~70 mAh g^{-1} at a current density of 400 mA g^{-1}. The Li-HEC is capable of delivering the energy and power densities of ~47 Wh kg^{-1} and ~1.6 kW kg^{-1}, respectively, between 0 and 3 V. In addition, Li_2CoPO_4F/AC, Li-HEC renders the good cyclability of about 30 000 cycles.

3.5. Silicates

3.5.1. Li_2MnSiO_4. Since the exploitation of polyanion framework material as potential electrode material in Li-ion batteries, the same concept has been employed to study the performance of Li-insertion-type electrode in Li-HEC applications. Among them, Li_2MnSiO_4 is found noteworthy due to its eco-friendliness and low cost; however, inherent conducting behavior and amorphousization of the material hinders the possibility of using them in practical applications.[147,148] However, the preparation of phase pure material is found complicated irrespective of the synthesis routes. Recently, Aravindan et al.[149−153] extensively investigated by various synthetic approaches and concluded that inclusion of more carbon alleviates said issues and can be used as electrode material for insertion-type electrode, although it offers reduction in volumetric capacity. In this line, Karthikeyan et al.[154] reported the possibility of using carbon-coated Li_2MnSiO_4 prepared by adipic acid-mediated solid-state reaction as insertion-type electrode along with AC. Usually the electrode prepared by said method delivered the reversible capacity of ~150 mAh g^{-1} between 1.5 and 4.8 V vs Li. In the hybrid configuration, Li_2MnSiO_4/AC Li-HEC delivered maximum energy and power densities of ~54 Wh kg^{-1} and ~1.5 kW kg^{-1}, respectively, between 0 and 3 V. Further, Li_2MnSiO_4/AC Li-HEC rendered good cyclability for about 1000 cycles and retained ~85% of the initial capacity.

3.5.2. Li_2FeSiO_4. Li_2FeSiO_4 is also another class of polyanion framework materials comprising orthorhombic structure, which is an analogue of Li_2MnSiO_4.[147,148] Electrochemical performance of the Li_2FeSiO_4 is found better in elevated temperature conditions, and several reports are available in the electrochemical performance, particularly Manthiram and co-workers' report.[155] The authors clearly point out that excellent reversibility of the $Fe^{3+/4+}$ redox couple

dx.doi.org/10.1021/cr5000915 | Chem. Rev. 2014, 114, 11619−11635

in the silicate matrix results in the possibility of achieving higher theoretical capacity of over 333 mAh g^{-1} with excellent cyclability. However, realizing the theoretical capacity is not possible for all of the materials, which depends on the nature of the material and synthetic procedures. In this line, Karthikeyan et al.[156] reported the possibility of utilizing carbon-coated orthorhombic Li_2FeSiO_4 particles prepared by the solid-state approach as insertion-type electrode in Li-HEC configuration along with AC. The Li_2FeSiO_4/AC system presented the maximum energy and power densities of ~43 Wh kg^{-1} and ~1.4 kW kg^{-1}, respectively. Good cycling profiles are also noted during cycling with ~89% capacitance retention after 1000 cycles between 0 and 3 V.

4. DISCUSSION

Apparent from the Ragone plot (Figure 11), it is clear that there are three materials, TiO_2, anatase, and bronze phases;

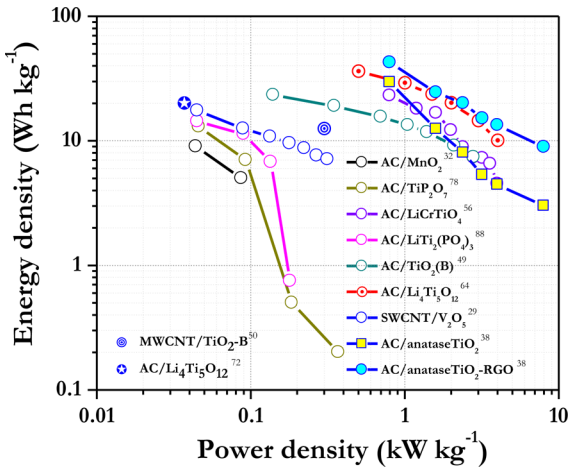

Figure 11. Ragone plot indicates the performance of various insertion-type anode materials tested for Li-HEC applications in nonaqueous medium. AC, activated carbon; MWCNT, multiwalled carbon nanotube; SWCNT, single walled carbon nanotube; RGO, reduced graphene oxide. The data points were collected from the superscripted references in the figure.

$LiCrTiO_4$ and $Li_4Ti_4O_{12}$ are found appealing and dominant as compared to the rest of the insertion-type anodes investigated for Li-HEC applications. Among the spinel phase, $Li_4Ti_4O_{12}$ exhibits favorable properties to be used in practical Li-HEC; there are still a few issues to be addressed, particularly the power density issues. To attain high power capability of Li-HEC, conductive coatings should be adopted; however, such coating certainly provides the reduction in volumetric capacitance and increase in production cost as well. However, metallic coatings/decoration, likely Au, Pd, and Ag, are other alternate solutions, but the cost is the serious debate here. To attain a desired goal, a conducting network is necessary to alleviate the intrinsic nature of the insertion-type compound. Carbon coating or making composites with carbonaceous materials such as CNTs and CNFs can be effectively utilized to improve the power capability of the electrode, because the Li-diffusion properties are found sluggish at high current rates. As a result, a dramatic improvement of such power density values after incorporating mentioned surface modifications is clearly demonstrated by Prof. Naoi's group even at 1200 C rate.[65] Recently, Li-HEC was commercially introduced into the market based on prelithiated graphite anode and high surface area AC anode. However, the main issue related to the negative electrode, that is, graphite, is that prelithiation results in the formation of SEI over the surface, which consumes a huge amount of Li during the first discharge, because Li-insertion takes place in well-ordered graphite below 0.2 V vs Li. This SEI formation results in an increase in the internal resistance of the system and subsequently hinders from achieving the desired power density. Therefore, construction of Li-HEC assembly is a two-step process while employing prelithiated graphite as anode, which is the main hurdle during mass production. Another insertion-type anode is spinel phase $LiCrTiO_4$, which exhibits slightly lower theoretical capacity than $Li_4Ti_4O_{12}$ for reversible Li-insertion. The Li-HEC configuration with AC cathode delivered more or less the same energy density values as compared to the former configuration. This is mainly due to the crystallographic arrangement, that is, spinel phase, which undergoes two-phase Li-insertion/extraction reaction during electrochemical cycling at relatively lower operating potential. Because of the toxicity of the Cr, not much work has been explored for this compound either in Li-HEC or in Li-ion battery configurations. Although the higher energy density is observed for pristine (~30 Wh kg^{-1}) and anatase TiO_2-RGO composite (~42 Wh kg^{-1}), the ICL, higher operating potential, and poor long-term cyclability are the issues for employing them in practical devices as compared to spinel anodes.[38] To overcome the said issues, another polymorph of TiO_2, bronze phase, is introduced, which exhibits more favorable characteristics like lower operating potential and negligible ICL that render it a prospective anode material for Li-ion batteries and Li-HEC applications. The performance of TiO_2-B as anode in Li-HEC is found comparable to that of both spinel phase $LiCrTiO_4$ and $Li_4Ti_5O_{12}$ anodes with AC counter electrode. Especially, all three electrodes delivered the same energy density at high current rates (delivers high power density), whereas low current rates spinel phase $Li_4Ti_5O_{12}$ is found superior as compared to $Li_4Ti_5O_{12}$. Moreover, confined carbon coating is a bit complicated for the case of TiO_2-B phase; however, such coating is necessary to improve the power density of the Li-HEC. To enable such ultrafine coating heat treatment above ~500 °C in inert atmosphere condition is necessary, but during that a temperature conversion of monoclinic phase to anatase phase could be inevitable. However, making composite with carbon results in a heterogeneous coating and also provides the suppression of volumetric capacitance as well. Moreover, cyclability is another important issue for TiO_2-B polymorph. Other insertion hosts, likely super cubic TiP_2O_7 and NASICON-type $LiTi_2(PO_4)_3$, exhibit almost the same operating potential (~2.6 V vs Li) and undergo the biphase Li-insertion/extraction process.[87] However, lower reversible capacity and higher operating potential are the main issues to incorporate them in practical Li-HEC. Apart from the said issues, performances of both polyanions (TiP_2O_7 and $LiTi_2(PO_4)_3$) are found inferior as compared to the lower operating potential anodes like spinel phase $LiCrTiO_4$ and $Li_4Ti_5O_{12}$. As expected, MnO_2 experiences the very least energy density among the insertion-type anode materials investigated. The observed values are consistent with previous values reported by other authors in the same Li-HEC configuration. This clearly showed that spinel phase $Li_4Ti_5O_{12}$ decorated with carbonaceous materials is the best choice to be used as insertion-type electrode used in Li-HEC along with either high surface area AC or graphene as counter electrode. Similar to the insertion-type anodes, there are several Li-

dx.doi.org/10.1021/cr5000915 | Chem. Rev. 2014, 114, 11619−11635

insertion-type cathode active materials explored for Li-HEC applications (Figure 12). The energy densities of insertion-type

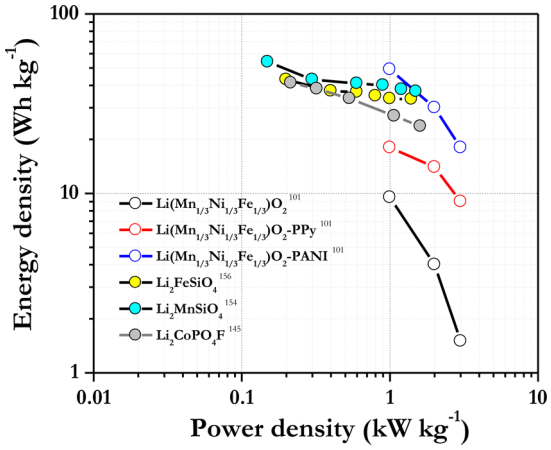

Figure 12. Ragone plot showing the performance of various insertion-type cathode materials tested for Li-HEC applications in nonaqueous medium. The data points were collected from the superscripted references in the figure.

cathode materials are performed better than anodes in Li-HEC configuration, which is mainly because of the higher redox potential of the transition metal oxide used. Long-term cyclability is very critical for Li-HEC, but achieving such cyclability is questionable for the case of cathodes. Most of the cathodes reported here are based on "Mn", which is soluble in the conventional carbonate-based electrolytes in the John–Teller region. On the contrary, recentl, Karthikeya et al.[145] reported the extraordinary cyclability of Co-based fluorophosphate, Li_2CoPO_4F, for about 30 000 cycles. These results clearly showed the promising feature of such cathodes for Li-HEC applications. However, the usage of such toxic and expensive transition metal Co is questionable during the mass production. Moreover, unlike that of $LiFePO_4$ and $LiMnPO_4$, in parent $LiCoPO_4$, dissolution of the $(PO_4)^{3-}$ group occurred due to the nucleophilic attack of F^- ions from HF on phosphorus atoms, particularly in delithiated state. Whether a similar kind of dissolution occurred in fluorophosphates is not known yet.[137,138] So, further studies are required to analyze such a system before reaching the commercialization. As expected, poor electrochemical performances are noted for the Fe-based layered-type cathodes of either Li-rich or stoichiometric compositions ($LiMn_{1/3}Ni_{1/3}Fe_{1/3}O_2$ and $Li_{1.2}(Mn_{0.32}Ni_{0.32}Fe_{0.16})O_2$), although it is finely decorated with conducting polymers like PPy and PANI due to the intrinsic nature of Fe.[157] This clearly showed any advancement in the insertion-type electrode completely depends on insertion-type anodes, rather than cathodes. Therefore, high capacity with low operating potential anodes is highly anticipated to fulfill the necessary demand to satisfy the requirements to drive zero emission transportation applications.

In Li-HEC, most of the research works are devoted to the development of insertion-type electrode; unfortunately, not much work has been carried out on the cathodic side. Generally, AC has been utilized as the unanimous choice as counter electrode in Li-HEC assembly. Although the AC has unique properties such as high specific surface area, electronic conductivity, thermal stability, excellent chemical stability with wide range of pH values, and cost-effectiveness, the performance characteristics of such electrode in aqueous and nonaqueous medium will be entirely different.[158] The performance of AC in Li-HEC is of an entirely different configuration than symmetric and asymmetric, so the performance of such an electrode should be investigated. Therefore, we are very much interested in studying the performance of AC electrode in Li-HEC assembly with commercially available spinel phase $Li_4Ti_5O_{12}$ anode (Sigma-Aldrich, U.S.). The commercially available AC (BET surface area 817 m^2 g^{-1}, Norit, Netherlands)/$Li_4Ti_5O_{12}$ Li-HEC configuration delivered the energy density of ~36 Wh kg^{-1}. The idea of utilizing biomass derived AC is another important area of research, especially for coconut shells. The AC obtained from the chemical activation in the hydrothermal carbonization and subsequent physical activation process (CS-ZHTP) delivered the maximum energy density of ~69 Wh kg^{-1} (Figure 13). The observed energy density is

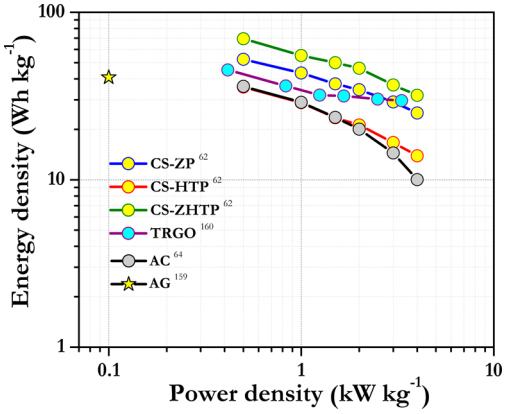

Figure 13. Ragone plot indicates the performance of spinel phase $Li_4Ti_5O_{12}$ insertion anode with various carbonaceous cathodes. AC, activated carbon; AG, activated graphene; TRGO, trigol reduced graphene oxide nanosheets; CS-ZP, coconut shell granules are treated with $ZnCl_2$ in the presence of CO_2; CS-HTP, coconut shell granules in hydrothermal treatment and pyrolyzed in the presence of CO_2 in succession; CS-ZHTP, coconut shell granules in hydrothermal reaction and pyrolyzed in the presence of CO_2 with addition of $ZnCl_2$. The data points were collected from the superscripted references in the figure.

almost 2 times higher than that of commercially available AC electrodes. It is generally believed that the chemical activation process at high temperature certainly suppresses the electrical conductivity of the carbonaceous materials, although it also enables high specific surface area and generates mesoporosity.[62] In the case of hydrothermal carbonization process, it certainly overcomes the issues mentioned and also generates a higher percentage of mesoporosity during subsequent pyrolysis (~60%). Without any chemical activation, hydrothermal and physical activation process yielded (CS-HTP) AC and delivered the same energy density of commercial AC (~36 Wh kg^{-1}), but exhibits excellent power capability as compared to commercial AC. Here, hydrothermal activation process is the trick to attain high power density. CS-ZP prepared with chemical and physical activation process alone translates more energy density (~52 Wh kg^{-1}) than commercial AC without any hydrothermal treatment. This clearly suggests that the activation process played a vital role with appropriate tuning for the enhancement of energy density. However, the recent boom on the graphene has also been investigated as a prospective cathode active material for Li-HEC. Stoller et al.[159] first reported the

dx.doi.org/10.1021/cr5000915 | Chem. Rev. 2014, 114, 11619–11635

utilization of KOH treated microwave exfoliated graphite oxide, shortly activated graphene (AG) in Li-HEC assembly, which delivered the energy density of ~40.8 Wh kg^{-1}. Without any activation process, trigol reduced graphene oxide (TRGO) delivered a much higher energy density (~45 Wh kg^{-1}) and rendered good cyclability as well.[160] Irrespective of the supercapacitor configuration (symmetric, asymmetric, and hybrid) and electrolyte medium (aqueous or nonaqueous), graphene-based systems performed better than conventional high surface area porous carbons and AC electrode. However, reproducibility of the results was a bit difficult, because the graphene prepared from batch to batch and synthesis technique to technique delivered different results.[161] As of now, the results obtained from such systems may be fascinating, but the scalability is another big issue. We believe AC derived from biomass precursors is the best choice to use in practical Li-HEC, particularly the hydrothermally treated one.

5. CONCLUSION

This Review clearly highlights various Li-insertion-type electrodes, that is, anode and cathode, used for the construction of high energy density Li-HEC with long cycle life in nonaqueous medium along with fundamental properties. The high surface area carbonaceous material, that is, activated carbon, was the unanimous. Although Li-insertion-type electrodes comprising Li-HEC delivered the highest energy density, the long-term cyclability is questionable. This poor cyclability is mainly because of the usage of transition metals like Mn, Ni, Co, and Fe predominantly in most of the cathodes, which has several issues with the electrolyte counterpart during the redox reactions. Therefore, much attention is paid to developing high performance Li-insertion anodes, preferably spinel $Li_4Ti_5O_{12}$ by considering its salient features. Unfortunately, the $Li_4Ti_5O_{12}$-based Li-HEC delivered less energy and power densities. As a result, several attempts were focused to search for the alternate insertion anode such as TiP_2O_2, $LiTi_2(PO_4)_3$, $LiCrTiO_4$, polymorphs of TiO_2, etc., but the results suggest $Li_4Ti_5O_{12}$ remains attractive. Therefore, surface modification with carbon nanostructures such as carbon coating, attaching to CNTs, and making composite with graphene, results in the dramatic improvement in the high power capability and energy density as well. Unlike that of research activities in Li-insertion components, no such work has been carried out on the counter electrode side, that is, carbonaceous materials. Recently, we initiated tailoring of the carbonaceous materials (trigol reduced graphene oxide nanosheets, coconut shell derived high surface area carbon) to further extend both energy and power densities.[62,160] Both attaching spinel particles into carbon nanofibers or CNTs and tailoring carbonaceous counter electrode are necessary to make high energy and power density Li-HEC for practical applications to drive EV and HEVs, thereby suppressing environmental pollution.

AUTHOR INFORMATION

Corresponding Authors

*E-mail: aravind_van@yahoo.com.
*E-mail: joeg@yardney.com.
*E-mail: leeys@chonnam.ac.kr.
*E-mail: madhavi@ntu.edu.sg.

Notes

The authors declare no competing financial interest.

Biographies

Vanchiappan Aravindan is currently working at the Energy Research Institute @ NTU (ERI@N), Nanyang Technological University, Singapore. He received his Ph.D. in 2009 at Gandhigram Rural University, Gandhigram, Tamilnadu, India. He then joined as a Post-Doctoral Fellow at The Research Institute for Catalysis, Chonnam National University, Gwang-ju, South Korea, with Prof. Yun-Sung Lee, Faculty of Applied Chemical Engineering. He moved in 2010 to the present organization to continue his research career. He has authored and coauthored over 100 peer-reviewed international publications to his credit. His research interests are mainly in the development of high performance electrode and electrolyte materials for Li-ion and post Li-ion batteries and supercapacitors. Web page: https://sites.google.com/site/vanchiappanaravindan/home.

Joseph Gnanaraj is the Senior Scientist at Yardney Technical Products Inc., East Greenwich, RI. He received his M.Phil from Bharathidasan University in 1990, and the research work was carried out at Central Electrochemical Research Institute, Karaikudi, India, under the guidance of Dr. Kuppusamy. He received Ph.D. in 1998 in Material Science and Electrochemistry from the University of Pune working with Prof. R. N. Karekar. He joined in 1999 as a Post-Doctoral Fellow and then in 2001 as a Senior Researcher with Professor Doron Aurbach, at Bar-Ilan University, Israel. He joined in 2003 at Worcester Polytechnic Institute, MA, as a Visiting Research Scientist. He has authored and coauthored over 60 peer-reviewed international publications and is an active member of the Electrochemical Society Inc. He is a manuscript reviewer for various international journals of electrochemistry and materials. His research interests are in the fields of Li-ion battery, electrode materials, organic electrolytes, and hybrid Li-ion/ultracapacitor systems.

Yun-Sung Lee is currently working as an Associate Professor at Chonnam National University, Gwang-ju, in Korea. He received his M.S. from Chonbuk National University in 1998, and the research work was carried out under the guidance of Prof. Kee-Suk Nahm. He received Ph.D. in 2001 in Applied Chemistry from Saga University in Japan under the direction of Prof. Masaki Yoshio. He joined in 2001 as a Post-Doctoral Fellow as Doctoral Researcher with Professor Yuichi Sato, at Kanagawa University in Japan. He joined in 2003 at Chonnam National University as an Assistant Professor. He has authored and coauthored over 140 peer-reviewed international publications and is an active member of the lithium secondary battery field. His research interests are in the fields of Li-ion battery, electrode materials, and hybrid capacitor systems. Web page: http://altair.chonnam.ac.kr/~leeys/eng.php.

Srinivasan Madhavi is currently an Associate Professor at the School of Materials Science and Engineering, Nanyang Technological University (NTU), Singapore. She graduated from Indian Institute of Technology (IIT), Chennai (India), and completed her Ph.D. from the National University of Singapore (Singapore). Her research interest is to enhance the performance of energy storage devices such as lithium ion batteries, supercapacitors, and advanced batteries with the help of multifunctional nanoscale materials to power printed electronics, to store energy from renewable sources, and for powering electric vehicles. Her focus is on the fabrication and investigation of nanoscale materials/architectures for electrochemical energy storage devices. Web page: http://Webserver.mse.ntu.edu.sg/homepages/madhavi/index.html.

ACKNOWLEDGMENTS

V.A. and S.M. thank the National Research foundation (NRF, Singapore) for financial support through the Competitive Research Programme (CRP) (Grant no. NRF-CRP4-2008-03). Y.-S.L. acknowledges the support from the International Cooperation of the Korea Institute of Energy Technology Evaluation and Planning (KETEP) grant funded by the Korea Government Ministry of Knowledge Economy (no. 20128510010050).

REFERENCES

(1) Yoo, H. D.; Markevich, E.; Salitra, G.; Sharon, D.; Aurbach, D. *Mater. Today* **2014**, *17*, 110.
(2) Naoi, K. *Electrochemistry* **2013**, *81*, 775.
(3) Naoi, K.; Ishimoto, S.; Miyamoto, J.-i.; Naoi, W. *Energy Environ. Sci.* **2012**, *5*, 9363.
(4) Plitz, I.; DuPasquier, A.; Badway, F.; Gural, J.; Pereira, N.; Gmitter, A.; Amatucci, G. G. *Appl. Phys. A: Mater. Sci. Process.* **2006**, *82*, 615.
(5) Amatucci, G. G.; Badway, F.; Du Pasquier, A.; Zheng, T. *J. Electrochem. Soc.* **2001**, *148*, A930.
(6) Naoi, K.; Simon, P. *Electrochem. Soc. Interface* **2008**, *17*, 34.
(7) Choi, N.-S.; Chen, Z.; Freunberger, S. A.; Ji, X.; Sun, Y.-K.; Amine, K.; Yushin, G.; Nazar, L. F.; Cho, J.; Bruce, P. G. *Angew. Chem., Int. Ed.* **2012**, *51*, 9994.
(8) Naoi, K.; Nagano, Y. *Supercapacitors*; Wiley-VCH Verlag GmbH & Co. KGaA: Weinheim, Germany, 2013; p 239.
(9) Aravindan, V.; Sundaramurthy, J.; Jain, A.; Kumar, P. S.; Ling, W. C.; Ramakrishna, S.; Srinivasan, M. P.; Madhavi, S. *ChemSusChem* **2014**, DOI: 10.1002/cssc.201400157.
(10) Pasquier, A. D.; Plitz, I.; Gural, J.; Badway, F.; Amatucci, G. G. *J. Power Sources* **2004**, *136*, 160.
(11) Cairns, E. J.; Albertus, P. *Annu. Rev. Chem. Biomol. Eng.* **2010**, *1*, 299.
(12) Simon, P.; Taberna, P.-L.; Béguin, F. *Supercapacitors*; Wiley-VCH Verlag GmbH & Co. KGaA: Weinheim, Germany, 2013; p 131.
(13) Pandolfo, T.; Ruiz, V.; Sivakkumar, S.; Nerkar, J. *Supercapacitors*; Wiley-VCH Verlag GmbH & Co. KGaA: Weinheim, Germany, 2013; p 69.
(14) Frackowiak, E.; Béguin, F. *Carbon* **2001**, *39*, 937.
(15) Béguin, F.; Presser, V.; Balducci, A.; Frackowiak, E. *Adv. Mater.* **2014**, *26*, 2219.
(16) Frackowiak, E. *Supercapacitors*; Wiley-VCH Verlag GmbH & Co. KGaA: Weinheim, Germany, 2013; p 207.
(17) Brousse, T.; Bélanger, D.; Guay, D. *Supercapacitors*; Wiley-VCH Verlag GmbH & Co. KGaA: Weinheim, Germany, 2013; p 257.
(18) Zaghib, K.; Goodenough, J. B.; Mauger, A.; Julien, C. *J. Power Sources* **2009**, *194*, 1021.
(19) Xu, K. *Chem. Rev.* **2004**, *104*, 4303.
(20) Aricò, A. S.; Bruce, P.; Scrosati, B.; Tarascon, J. M.; Van Schalkwijk, W. *Nat. Mater.* **2005**, *4*, 366.
(21) Amine, K.; Yasuda, H.; Yamachi, M. *J. Power Sources* **1999**, *81*−*82*, 221.
(22) Cheng, L.; Li, H.-q.; Xia, Y.-y. *J. Solid State Electrochem.* **2006**, *10*, 405.
(23) Chernova, N. A.; Roppolo, M.; Dillon, A. C.; Whittingham, M. S. *J. Mater. Chem.* **2009**, *19*, 2526.
(24) Cheah, Y. L.; von Hagen, R.; Aravindan, V.; Fiz, R.; Mathur, S.; Madhavi, S. *Nano Energy* **2013**, *2*, 57.
(25) Cheah, Y. L.; Gupta, N.; Pramana, S. S.; Aravindan, V.; Wee, G.; Srinivasan, M. *J. Power Sources* **2011**, *196*, 6465.
(26) Cheah, Y. L.; Aravindan, V.; Madhavi, S. *J. Electrochem. Soc.* **2012**, *159*, A273.
(27) Cheah, Y. L.; Aravindan, V.; Madhavi, S. *ACS Appl. Mater. Interfaces* **2013**, *5*, 3475.
(28) Cheah, Y. L.; Aravindan, V.; Madhavi, S. *J. Electrochem. Soc.* **2013**, *160*, A1016.
(29) Aravindan, V.; Cheah, Y. L.; Mak, W. F.; Wee, G.; Chowdari, B. V. R.; Madhavi, S. *ChemPlusChem* **2012**, *77*, 570.
(30) Julien, C. M.; Massot, M.; Poinsignon, C. *Spectrochim. Acta, Part A* **2004**, *60*, 689.
(31) Xu, C.; Kang, F.; Li, B.; Du, H. *J. Mater. Res.* **2012**, *25*, 1421.

(32) Aravindan, V.; Reddy, M.; Madhavi, S.; Rao, G.; Chowdari, B. *Nanosci. Nanotechnol. Lett.* **2012**, *4*, 724.
(33) Wang, G.-X.; Zhang, B.-L.; Yu, Z.-L.; Qu, M.-Z. *Solid State Ionics* **2005**, *176*, 1169.
(34) Kavan, L. *Chem. Rec.* **2012**, *12*, 131.
(35) Zhang, X.; Aravindan, V.; Kumar, P. S.; Liu, H.; Sundaramurthy, J.; Ramakrishna, S.; Madhavi, S. *Nanoscale* **2013**, *5*, 5973.
(36) Zhang, X.; Suresh Kumar, P.; Aravindan, V.; Liu, H. H.; Sundaramurthy, J.; Mhaisalkar, S. G.; Duong, H. M.; Ramakrishna, S.; Madhavi, S. *J. Phys. Chem. C* **2012**, *116*, 14780.
(37) Suresh Kumar, P.; Aravindan, V.; Sundaramurthy, J.; Thavasi, V.; Mhaisalkar, S. G.; Ramakrishna, S.; Madhavi, S. *RSC Adv.* **2012**, *2*, 7983.
(38) Kim, H.; Cho, M.-Y.; Kim, M.-H.; Park, K.-Y.; Gwon, H.; Lee, Y.; Roh, K. C.; Kang, K. *Adv. Energy Mater.* **2013**, *3*, 1500.
(39) Cai, Y.; Zhao, B.; Wang, J.; Shao, Z. *J. Power Sources* **2014**, *253*, 80.
(40) Shin, J.-Y.; Samuelis, D.; Maier, J. *Adv. Funct. Mater.* **2011**, *21*, 3464.
(41) Aravindan, V.; Shubha, N.; Cheah, Y. L.; Prasanth, R.; Chuiling, W.; Prabhakar, R. R.; Madhavi, S. *J. Mater. Chem. A* **2013**, *1*, 308.
(42) Brutti, S.; Gentili, V.; Menard, H.; Scrosati, B.; Bruce, P. G. *Adv. Energy Mater.* **2012**, *2*, 322.
(43) Armstrong, A. R.; Armstrong, G.; Canales, J.; García, R.; Bruce, P. G. *Adv. Mater.* **2005**, *17*, 862.
(44) Armstrong, G.; Armstrong, A. R.; Bruce, P. G.; Reale, P.; Scrosati, B. *Adv. Mater.* **2006**, *18*, 2597.
(45) Armstrong, A. R.; Armstrong, G.; Canales, J.; Bruce, P. G. *Angew. Chem., Int. Ed.* **2004**, *43*, 2286.
(46) Ren, Y.; Liu, Z.; Pourpoint, F.; Armstrong, A. R.; Grey, C. P.; Bruce, P. G. *Angew. Chem., Int. Ed.* **2012**, *51*, 2164.
(47) Armstrong, G.; Armstrong, A. R.; Canales, J.; Bruce, P. G. *Chem. Commun.* **2005**, 2454.
(48) Armstrong, A. R.; Armstrong, G.; Canales, J.; Bruce, P. G. *J. Power Sources* **2005**, *146*, 501.
(49) Aravindan, V.; Shubha, N.; Ling, W. C.; Madhavi, S. *J. Mater. Chem. A* **2013**, *1*, 6145.
(50) Wang, Q.; Wen, Z. H.; Li, J. H. *Adv. Funct. Mater.* **2006**, *16*, 2141.
(51) Chen, F.; Li, R.; Hou, M.; Liu, L.; Wang, R.; Deng, Z. *Electrochim. Acta* **2005**, *51*, 61.
(52) Villevieille, C.; Van Thournout, M.; Scoyer, J.; Tessier, C.; Olivier-Fourcade, J.; Jumas, J. C.; Monconduit, L. *Electrochim. Acta* **2010**, *55*, 7080.
(53) Cho, W.; Kashiwagi, T.; Ra, W.; Nakayama, M.; Wakihara, M.; Kobayashi, Y.; Miyashiro, H. *Electrochim. Acta* **2009**, *54*, 1842.
(54) Cho, W.; Park, M.-S.; Kim, J.-H.; Kim, Y.-J. *Electrochim. Acta* **2012**, *63*, 263.
(55) Aravindan, V.; Ling, W. C.; Madhavi, S. *ChemPhysChem* **2012**, *13*, 3263.
(56) Aravindan, V.; Chuiling, W.; Madhavi, S. *J. Mater. Chem.* **2012**, *22*, 16026.
(57) Ohzuku, T.; Tatsumi, K.; Matoba, N.; Sawai, K. *J. Electrochem. Soc.* **2000**, *147*, 3592.
(58) Mukai, K.; Ariyoshi, K.; Ohzuku, T. *J. Power Sources* **2005**, *146*, 213.
(59) Patoux, S.; Masquelier, C. *Chem. Mater.* **2002**, *14*, 5057.
(60) Ooms, F. G. B.; Kelder, E. M.; Schoonman, J.; Wagemaker, M.; Mulder, F. M. *Solid State Ionics* **2002**, *152−153*, 143.
(61) Yang, Z.; Choi, D.; Kerisit, S.; Rosso, K. M.; Wang, D.; Zhang, J.; Graff, G.; Liu, J. *J. Power Sources* **2009**, *192*, 588.
(62) Jain, A.; Aravindan, V.; Jayaraman, S.; Kumar, P. S.; Balasubramanian, R.; Ramakrishna, S.; Madhavi, S.; Srinivasan, M. *Sci. Rep.* **2013**, *3*, Art. No. 3002.
(63) Banerjee, A.; Upadhyay, K. K.; Puthusseri, D.; Aravindan, V.; Madhavi, S.; Ogale, S. *Nanoscale* **2014**, *6*, 4387.
(64) Puthusseri, D.; Aravindan, V.; Madhavi, S.; Ogale, S. *Electrochim. Acta* **2014**, *130*, 766.
(65) Naoi, K.; Naoi, W.; Aoyagi, S.; Miyamoto, J.-i.; Kamino, T. *Acc. Chem. Res.* **2013**, *46*, 1075.
(66) Naoi, K.; Ishimoto, S.; Isobe, Y.; Aoyagi, S. *J. Power Sources* **2010**, *195*, 6250.
(67) Yi, T.-F.; Jiang, L.-J.; Shu, J.; Yue, C.-B.; Zhu, R.-S.; Qiao, H.-B. *J. Phys. Chem. Solids* **2010**, *71*, 1236.
(68) Su, X.; Wu, Q.; Zhan, X.; Wu, J.; Wei, S.; Guo, Z. *J. Mater. Sci.* **2012**, *47*, 2519.
(69) Zhu, G.-N.; Wang, Y.-G.; Xia, Y.-Y. *Energy Environ. Sci.* **2012**, *5*, 6652.
(70) Naoi, K. *Fuel Cells* **2010**, *10*, 825.
(71) Chen, Z.; Belharouak, I.; Sun, Y. K.; Amine, K. *Adv. Funct. Mater.* **2013**, *23*, 959.
(72) Ni, J.; Yang, L.; Wang, H.; Gao, L. *J. Solid State Electrochem.* **2012**, *16*, 2791.
(73) Kim, H.; Park, K.-Y.; Cho, M.-Y.; Kim, M.-H.; Hong, J.; Jung, S.-K.; Roh, K. C.; Kang, K. *ChemElectroChem* **2014**, *1*, 125.
(74) Cheng, L.; Liu, H.-J.; Zhang, J.-J.; Xiong, H.-M.; Xia, Y.-Y. *J. Electrochem. Soc.* **2006**, *153*, A1472.
(75) Jung, H.-G.; Venugopal, N.; Scrosati, B.; Sun, Y.-K. *J. Power Sources* **2013**, *221*, 266.
(76) Barpanda, P.; Nishimura, S.-i.; Yamada, A. *Adv. Energy Mater.* **2012**, *2*, 841.
(77) Masquelier, C.; Croguennec, L. *Chem. Rev.* **2013**, *113*, 6552.
(78) Aravindan, V.; Reddy, M. V.; Madhavi, S.; Mhaisalkar, S. G.; Subba Rao, G. V.; Chowdari, B. V. R. *J. Power Sources* **2011**, *196*, 8850.
(79) Uebou, Y.; Okada, S.; Egashira, M.; Yamaki, J.-I. *Solid State Ionics* **2002**, *148*, 323.
(80) Shi, Z.; Wang, Q.; Ye, W.; Li, Y.; Yang, Y. *Microporous Mesoporous Mater.* **2006**, *88*, 232.
(81) Kishore, M. S.; Pralong, V.; Caignaert, V.; Varadaraju, U. V.; Raveau, B. *J. Power Sources* **2007**, *169*, 355.
(82) Kosova, N. V.; Osintsev, D. I.; Uvarov, N. F.; Devyatkina, E. T. *Chem. Sustainable Dev.* **2005**, *13*, 253.
(83) Goodenough, J. B.; Kim, Y. *Chem. Mater.* **2009**, *22*, 587.
(84) Gong, Z.; Yang, Y. *Energy Environ. Sci.* **2011**, *4*, 3223.
(85) Aravindan, V.; Chuiling, W.; Madhavi, S. *RSC Adv.* **2012**, *2*, 7534.
(86) Arun, N.; Aravindan, V.; Ling, W. C.; Madhavi, S. *J. Alloys Compd.* **2014**, *603*, 48.
(87) Aravindan, V.; Ling, W. C.; Hartung, S.; Bucher, N.; Madhavi, S. *Chem.—Asian J.* **2014**, *9*, 878.
(88) Aravindan, V.; Chuiling, W.; Reddy, M. V.; Rao, G. V. S.; Chowdari, B. V. R.; Madhavi, S. *Phys. Chem. Chem. Phys.* **2012**, *14*, 5808.
(89) Prem Kumar, T.; Sri Devi Kumari, T.; Manuel Stephan, A. *J. Indian Inst. Sci.* **2009**, *89*, 393.
(90) Kaskhedikar, N. A.; Maier, J. *Adv. Mater.* **2009**, *21*, 2664.
(91) Shukla, A. K.; Prem Kumar, T. *Curr. Sci.* **2008**, *94*, 314.
(92) Yoshio, M.; Nakamura, H.; Wang, H. *Electrochem. Solid-State Lett.* **2006**, *9*, A561.
(93) Aida, T.; Yamada, K.; Morita, M. *Electrochem. Solid-State Lett.* **2006**, *9*, A534.
(94) Khomenko, V.; Raymundo-Piñero, E.; Béguin, F. *J. Power Sources* **2008**, *177*, 643.
(95) Sivakkumar, S. R.; Pandolfo, A. G. *Electrochim. Acta* **2012**, *65*, 280.
(96) Kim, J.-H.; Kim, J.-S.; Lim, Y.-G.; Lee, J.-G.; Kim, Y.-J. *J. Power Sources* **2011**, *196*, 10490.
(97) Cao, W. J.; Zheng, J. P. *J. Power Sources* **2012**, *213*, 180.
(98) Lee, J. H.; Shin, W. H.; Ryou, M.-H.; Jin, J. K.; Kim, J.; Choi, J. W. *ChemSusChem* **2012**, *5*, 2328.
(99) Cao, W. J.; Shih, J.; Zheng, J. P.; Doung, T. *J. Power Sources* **2014**, *257*, 388.
(100) Gardiner, G. R.; Islam, M. S. *Chem. Mater.* **2009**, *22*, 1242.
(101) Karthikeyan, K.; Amaresh, S.; Aravindan, V.; Kim, H.; Kang, K. S.; Lee, Y. S. *J. Mater. Chem. A* **2013**, *1*, 707.
(102) Ohzuku, T.; Makimura, Y. *Chem. Lett.* **2001**, 744.

(103) Yoon, J. H.; Bang, H. J.; Prakash, J.; Sun, Y. K. *Mater. Chem. Phys.* **2008**, *110*, 222.
(104) James, A. C. W. P.; Goodenough, J. B. *J. Solid State Chem.* **1988**, *76*, 87.
(105) Kobayashi, H.; Tabuchi, M.; Shikano, M.; Yasuo, N.; Kageyama, H.; Ishida, T.; Nakamura, H.; Kurioka, Y.; Kanno, R. *J. Power Sources* **1999**, *81−82*, 524.
(106) Park, K.-S.; Im, D.; Benayad, A.; Dylla, A.; Stevenson, K. J.; Goodenough, J. B. *Chem. Mater.* **2012**, *24*, 2673.
(107) Park, M.-S.; Lim, Y.-G.; Kim, J.-H.; Kim, Y.-J.; Cho, J.; Kim, J.-S. *Adv. Energy Mater.* **2011**, *1*, 1002.
(108) Park, M.-S.; Lim, Y.-G.; Park, J.-W.; Kim, J.-S.; Lee, J.-W.; Kim, J. H.; Dou, S. X.; Kim, Y.-J. *J. Phys. Chem. C* **2013**, *117*, 11471.
(109) Park, O. K.; Cho, Y.; Lee, S.; Yoo, H.-C.; Song, H.-K.; Cho, J. *Energy Environ. Sci.* **2011**, *4*, 1621.
(110) Jayaraman, S.; Aravindan, V.; Suresh Kumar, P.; Ling, W. C.; Ramakrishna, S.; Madhavi, S. *Chem. Commun.* **2013**, *49*, 6677.
(111) Jayaraman, S.; Aravindan, V.; Suresh Kumar, P.; Chui Ling, W.; Ramakrishna, S.; Madhavi, S. *ACS Appl. Mater. Interfaces* **2014**, *6*, 8660.
(112) Aravindan, V.; Sundaramurthy, J.; Kumar, P. S.; Shubha, N.; Ling, W. C.; Ramakrishna, S.; Madhavi, S. *Nanoscale* **2013**, *5*, 10636.
(113) Ma, S.-B.; Nam, K.-W.; Yoon, W.-S.; Yang, X.-Q.; Ahn, K.-Y.; Oh, K.-H.; Kim, K.-B. *Electrochem. Commun.* **2007**, *9*, 2807.
(114) Cericola, D.; Ruch, P. W.; Kötz, R.; Novák, P.; Wokaun, A. *Electrochem. Commun.* **2010**, *12*, 812.
(115) Cericola, D.; Novák, P.; Wokaun, A.; Kötz, R. *Electrochim. Acta* **2011**, *56*, 1288.
(116) Cericola, D.; Novák, P.; Wokaun, A.; Kötz, R. *J. Power Sources* **2011**, *196*, 10305.
(117) Hu, X.; Deng, Z.; Suo, J.; Pan, Z. *J. Power Sources* **2009**, *187*, 635.
(118) Manthiram, A.; Chemelewski, K.; Lee, E.-S. *Energy Environ. Sci.* **2014**, *7*, 1339.
(119) Santhanam, R.; Rambabu, B. *J. Power Sources* **2010**, *195*, 5442.
(120) Kim, M.; Kim, S.; Aravindan, V.; Kim, W.; Lee, S.; Lee, Y. *J. Electrochem. Soc.* **2013**, *160*, A1003.
(121) Kim, M. C.; Nam, K.-W.; Hu, E.; Yang, X.-Q.; Kim, H.; Kang, K.; Aravindan, V.; Kim, W.-S.; Lee, Y.-S. *ChemSusChem* **2014**, *7*, 829.
(122) Li, H.; Cheng, L.; Xia, Y. *Electrochem. Solid-State Lett.* **2005**, *8*, A433.
(123) Wu, H.; Rao, C. V.; Rambabu, B. *Mater. Chem. Phys.* **2009**, *116*, 532.
(124) Padhi, A. K.; Nanjundaswamy, K. S.; Goodenough, J. B. *J. Electrochem. Soc.* **1997**, *144*, 1188.
(125) Aravindan, V.; Gnanaraj, J.; Lee, Y.-S.; Madhavi, S. *J. Mater. Chem. A* **2013**, *1*, 3518.
(126) Son, C.; Yang, H.; Lee, G.; Cho, A.; Aravindan, V.; Kim, H.; Kim, W.; Lee, Y. *J. Alloys Compd.* **2011**, *509*, 1279.
(127) Goodenough, J. B.; Kim, Y. *Chem. Mater.* **2009**, *22*, 587.
(128) Goodenough, J. B. *J. Power Sources* **2007**, *174*, 996.
(129) Yuan, L.-X.; Wang, Z.-H.; Zhang, W.-X.; Hu, X.-L.; Chen, J.-T.; Huang, Y.-H.; Goodenough, J. B. *Energy Environ. Sci.* **2011**, *4*, 269.
(130) Wu, X.-L.; Jiang, L.-Y.; Cao, F.-F.; Guo, Y.-G.; Wan, L.-J. *Adv. Mater.* **2009**, *21*, 2710.
(131) Chen, S.; Hu, H.; Wang, C.; Wang, G.; Yin, J.; Cao, D. *J. Renewable Sustainable Energy* **2012**, *4*, 033114.
(132) Hu, X.; Huai, Y.; Lin, Z.; Suo, J.; Deng, Z. *J. Electrochem. Soc.* **2007**, *154*, A1026.
(133) Hu, X. B.; Lin, Z. J.; Liu, L.; Huai, Y. J.; Deng, Z. H. *J. Serb. Chem. Soc.* **2010**, *75*, 1259.
(134) Ping, L.; Zheng, J.; Shi, Z.; Qi, J.; Wang, C. *Chin. Sci. Bull.* **2013**, *58*, 689.
(135) Aravindan, V.; Gnanaraj, J.; Madhavi, S.; Liu, H.-K. *Chem.—Eur. J.* **2011**, *17*, 14326.
(136) Amine, K.; Yasuda, H.; Yamachi, M. *Electrochem. Solid-State Lett.* **2000**, *3*, 178.
(137) Markevich, E.; Sharabi, R.; Gottlieb, H.; Borgel, V.; Fridman, K.; Salitra, G.; Aurbach, D.; Semrau, G.; Schmidt, M. A.; Schall, N.; Bruenig, C. *Electrochem. Commun.* **2012**, *15*, 22.
(138) Sharabi, R.; Markevich, E.; Borgel, V.; Salitra, G.; Gershinsky, G.; Aurbach, D.; Semrau, G.; Schmidt, M. A.; Schall, N.; Stinner, C. *J. Power Sources* **2012**, *203*, 109.
(139) Yang, S. M. G.; Aravindan, V.; Cho, W. I.; Chang, D. R.; Kim, H. S.; Lee, Y. S. *J. Electrochem. Soc.* **2012**, *159*, A1013.
(140) Aravindan, V.; Cheah, Y. L.; Ling, W. C.; Madhavi, S. *J. Electrochem. Soc.* **2012**, *159*, A1435.
(141) Jang, I. C.; Son, C. G.; Yang, S. M. G.; Lee, J. W.; Cho, A. R.; Aravindan, V.; Park, G. J.; Kang, K. S.; Kim, W. S.; Cho, W. I.; Lee, Y. S. *J. Mater. Chem.* **2011**, *21*, 6510.
(142) Jang, I. C.; Lim, H.; Lee, S.; Karthikeyan, K.; Aravindan, V.; Kang, K.; Yoon, W.; Cho, W.; Lee, Y. *J. Alloys Compd.* **2010**, *497*, 321.
(143) Vasanthi, R.; Kalpana, D.; Renganathan, N. *J. Solid State Electrochem.* **2008**, *12*, 961.
(144) Amaresh, S.; Kim, G. J.; Karthikeyan, K.; Aravindan, V.; Chung, K. Y.; Cho, B. W.; Lee, Y. S. *Phys. Chem. Chem. Phys.* **2012**, *14*, 11904.
(145) Karthikeyan, K.; Amaresh, S.; Kim, K. J.; Kim, S. H.; Chung, K. Y.; Cho, B. W.; Lee, Y. S. *Nanoscale* **2013**, *5*, 5958.
(146) Okada, S.; Ueno, M.; Uebou, Y.; Yamaki, J.-i. *J. Power Sources* **2005**, *146*, 565.
(147) Boulineau, A.; Sirisopanaporn, C.; Dominko, R.; Armstrong, A. R.; Bruce, P. G.; Masquelier, C. *Dalton Trans.* **2010**, *39*, 6310.
(148) Islam, M. S.; Dominko, R.; Masquelier, C.; Sirisopanaporn, C.; Armstrong, A. R.; Bruce, P. G. *J. Mater. Chem.* **2011**, *21*, 9811.
(149) Aravindan, V.; Karthikeyan, K.; Amaresh, S.; Lee, Y. S. *Electrochem. Solid-State Lett.* **2011**, *14*, A33.
(150) Aravindan, V.; Ravi, S.; Kim, W. S.; Lee, S. Y.; Lee, Y. S. *J. Colloid Interface Sci.* **2011**, *355*, 472.
(151) Aravindan, V.; Karthikeyan, K.; Kang, K. S.; Yoon, W. S.; Kim, W. S.; Lee, Y. S. *J. Mater. Chem.* **2011**, *21*, 2470.
(152) Aravindan, V.; Karthikeyan, K.; Ravi, S.; Amaresh, S.; Kim, W. S.; Lee, Y. S. *J. Mater. Chem.* **2010**, *20*, 7340.
(153) Aravindan, V.; Karthikeyan, K.; Lee, J. W.; Madhavi, S.; Lee, Y. S. *J. Phys. D: Appl. Phys.* **2011**, *44*, 152001.
(154) Karthikeyan, K.; Aravindan, V.; Lee, S. B.; Jang, I. C.; Lim, H. H.; Park, G. J.; Yoshio, M.; Lee, Y. S. *J. Power Sources* **2010**, *195*, 3761.
(155) Muraliganth, T.; Stroukoff, K. R.; Manthiram, A. *Chem. Mater.* **2010**, *22*, 5754.
(156) Karthikeyan, K.; Aravindan, V.; Lee, S. B.; Jang, I. C.; Lim, H. H.; Park, G. J.; Yoshio, M.; Lee, Y. S. *J. Alloys Compd.* **2010**, *504*, 224.
(157) Okada, S.; Yamaki, J.-i. *J. Ind. Eng. Chem.* **2004**, *10*, 1104.
(158) Karthikeyan, K.; Amaresh, S.; Lee, S. N.; Sun, X.; Aravindan, V.; Lee, Y.-G.; Lee, Y. S. *ChemSusChem* **2014**, *7*, 1435.
(159) Stoller, M. D.; Murali, S.; Quarles, N.; Zhu, Y.; Potts, J. R.; Zhu, X.; Ha, H.-W.; Ruoff, R. S. *Phys. Chem. Chem. Phys.* **2012**, *14*, 3388.
(160) Aravindan, V.; Mhamane, D.; Ling, W. C.; Ogale, S.; Madhavi, S. *ChemSusChem* **2013**, *6*, 2240.
(161) Vargas, C. O. A.; Caballero, A.; Morales, J. *Nanoscale* **2012**, *4*, 2083.